The temperature influence in the photovoltaic panels performance

João Pedro Macedo Caleiro

Thesis to obtain the Master of Science Degree in

Electrical and Computer Engineering

Supervisor(s): Prof. Carlos Alberto Ferreira Fernandes

Prof. João Paulo Neto Torres

Examination Committee

Chairperson: Prof. Francisco André Corrêa Alegria

Supervisor: Prof. João Paulo Neto Torres

Member of the Committee: Prof. Paulo José da Costa Branco

March 2021

Declaration

I declare that this document is an original work of my own authorship and that it fulfils all the requirements of the Code of Conduct and Good Practices of the Universidade de Lisboa.

Acknowledgements

I would like to thank my dissertation coordinator, Prof. Carlos Fernandes, for giving me a vote of confidence and accepting my application for this dissertation. I would like to thank my dissertation coordinator, Prof. João Torres, for his willingness to discuss my doubts, giving suggestions, and providing feedback which proved important to the completion of this thesis. Lastly, I would also like to thank my parents for giving me the opportunity to finish my master's degree.

Resumo

Esta dissertação investiga o efeito que a temperatura irá ter nas células solares. Usando um software de análise de elementos finitos, várias simulações computacionais foram feitas de forma a poder estudar este efeito. As simulações feitas para células de silício, de telureto de cádmio, CIGS e de perovskita mostram que, de todas as células, as células de perovskita são as menos afetadas pela temperatura. Em termos das propriedades do silício, notou-se que o decréscimo que a banda proibida sofre com o aumento de temperatura irá provocar um decréscimo no valor da tensão de circuito aberto, o que irá provocar uma variação no seu coeficiente de temperatura de -0.37 %/ºC para -0.41 %/ºC, o que irá negativamente afetar a potência máxima e a eficiência da célula. Por outro lado, o acréscimo no índice de extinção, com a temperatura, irá levar a um aumento no valor da corrente de curto circuito, cujo coeficiente de temperatura irá crescer de 0.005 %/ºC para 0.03 %/ºC, o que será benéfico para o desempenho da célula. Paralelamente, um estudo de várias tecnologias de arrefecimento de sistemas fotovoltaicos foi feito, onde vantagens e desvantagens de cada método são discutidas.

Palavras-Chave: Células Solares; Temperatura; Semiconductores; Arrefecimento.

Abstract

This master thesis investigates the effect the temperature will have on solar cells. Using a finite element simulation software, several computational simulations were made in order to study this effect. The simulations made for silicon, CIGS, CdTe and perovskite cells show that, out of all the cells, perovskite cells are the least negatively affected by an increase in temperature. In terms of the silicon's properties, it has been found that the decrease in band gap with the temperature will cause a decrease in the value of the open circuit voltage of the cell, which will cause its temperature coefficient to go from -0.37 %/ºC to -0.41 %/ºC, which negatively impacts the maximum power and efficiency of the cell. The increase in the extinction index with the temperature, on the other hand, will lead to an increase in the short circuit current, which will grow from 0.005 %/ºC to 0.03 %/ºC, which will prove beneficial to the performance of the cell. Alongside this, a study of various cooling technologies was also conducted, where advantages and drawbacks of each method are discussed.

Keywords: Solar Cells; Temperature; Semiconductors; Cooling.

Table of Contents

List of Figures

List of Tables

List of Symbols

c	Speed of light in vacuum
E	Electric field
E_G	Band gap
G	Irradiance
I	Current
I_{pv}	Light generated current
I_S	Reverse saturation current
I_{SC}	Short circuit current
FF	Fill factor
h	Plank's constant
k	Boltzmann's constant
k	Extinction index
m_e^*	Effective mass of electron
m_h^*	Effective mass of hole
n	Diode ideality factor
n	Electron density
n	Refractive index
N_C	Effective density of states in conduction band
N_V	Effective density of states in valence band
n_i	Intrinsic carrier concentration
P	Power
P_{MP}	Maximum power
p	Hole density
q	Electron's charge
R_S	Series resistance
R_{SH}	Shunt resistance
T	Temperature
T_{AMB}	Ambient temperature
T_{CELL}	Cell temperature
V	Voltage
V_{OC}	Open circuit voltage
V_T	Thermal voltage

η	Efficiency
λ	Wavelenght
σ	Stefan–Boltzmann constant

List of Abbreviations

1D	One dimensional
2D	Two dimensional
a-Si	Amorphous silicon
CdTe	Cadmium telluride
CIS	Copper indium selenide
CIGS	Copper indium gallium selenide
CZTS	Copper zinc tin sulfide
DSSC	Dye-sensitized solar cells
I-V	Current-Voltage
mono-Si	Monocrystalline silicon
MJ	Multi-junction
NOCT	Nominal operating cell temperature
P-V	Power-Voltage
PCM	Phase change material
PV	Photovoltaic
PV/T	Photovoltaic/thermal
PSC	Perovskite solar cell
QD	Quantum dot
QDSC	Quantum dot solar cell
SJ	Single-junction
STC	Standard test conditions
TEC	Thermoelectric cooling

1. Introduction

An increase in the human population and human activity has led to an increase in the world energy consumption and global energy demand. Fossil fuels, which make up most of the world's energy use, pose problems due to their limited availability, their rising prices, and their negative impact on the environment, such as the emission of carbon dioxide. In order to combat this, there has been a growing interest in the development and use of renewable energy.

Solar energy has proven to be a renewable energy source that has many advantages as well as some drawbacks. It can be used either for the conversion of sunlight into electricity (as is the case in photovoltaic systems), or to generate heat (using some kind of concentrated solar power system). Solar energy, and photovoltaic systems in specific, can have many different applications such as the distillation of water, the powering of space satellites and the production of electricity for isolated areas that do not have access to the power grid. Its principal drawbacks are the relatively high cost of the equipment of the solar system, (such as the solar panels, the inverter, the wiring, and the batteries) and the amount of space that is required for the installation of the system. One of its main benefits, is that it can be harnessed, during the daytime, in every part of the globe, although the efficiency of the process will vary depending on the weather conditions of the local such as the temperature, the irradiance, the wind speed and the cloud opacity. Because of this, consideration must be taken about where to install the solar system responsible for the conversion of sunlight into electricity.

1.1 Motivation

The installed capacity of solar energy has increased in size in the last few years, with photovoltaics, in particular, having experienced an almost exponential growth as can be seen in Figure 1.1.

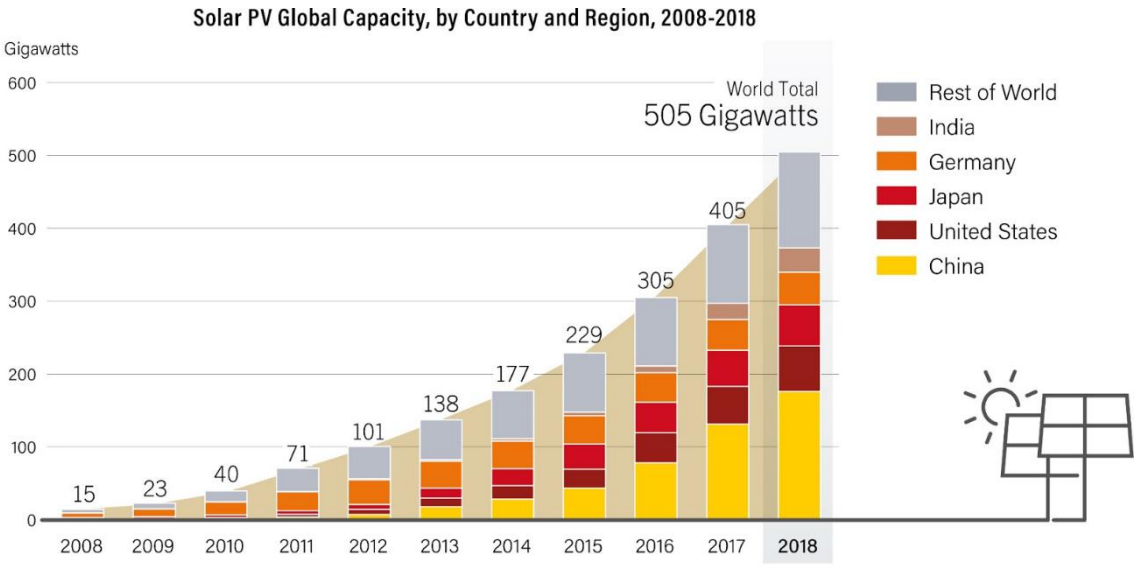

Figure 1.1 Global growth of the installed capacity of photovoltaics between 2008 and 2018 [1]

Aligned with this, there has also been considerable developments in photovoltaic technology, in the form of increased solar panel efficiencies, expected longevity of the panels and solar cell design, making photovoltaics an increasingly popular and in demand form of energy conversion. In order to maximize the efficiency of the photovoltaic system it is important to understand in what ways the weather conditions will influence the behavior of the panel.

Temperature is one of the more important factors that have an effect on the performance of solar panels since the majority of the absorbed sunlight that hits the photovoltaic system will be converted into heat, rather than into electricity. The heat generated in the solar panels will increase its temperature, thereby reducing the voltage generated and consequently the output power and efficiency. The increase in temperature may also result in an increase of the degradation rate of the panel and a lowering of the panel's lifetime.

Because of the negative impact the temperature will have on the performance of photovoltaic systems, it is crucial to better understand not only the underlying dynamics behind this effect, but also to study how to best counteract it by studying how the temperature will impact different types of solar cells, different solar cell's parameters and what cooling methods may be employed to lower the temperature of the panel.

1.2 Objectives

The main objective of this master thesis is the study of how the temperature negatively impacts the performance of solar cells, both from a theoretical and experimental perspective. Specific objectives include:

- A review of the literature where the impact the increase in temperature will have on different types of solar cells is studied;
- Explanation of the processes that occur in the operation of solar cells that lead to the temperature having a negative effect on their performance;
- Comparison of the temperature effect on the behavior of different types of solar cells, by means of computational simulations;
- Study of how certain solar cell's properties will change with the temperature and how those changes will affect the overall behavior of the cell;
- Development of one- and two-dimensional models of silicon solar cells and comparison between the two about how the temperature will affect their performance;
- A review of various cooling methods that may be used to cool photovoltaic systems and improve their performance. Comparisons between the different methods in terms of complexity, cost and efficiency are made.

1.3 Dissertation Outline

This dissertation is divided into 6 chapters which are described as follows:

- Chapter 1 – Introduction to the subject of the master thesis is done. The motivation, main objectives and the dissertation outline are presented;
- Chapter 2 – A review of the state of the art is conducted, where the impact of the temperature on different types of solar cells is studied;
- Chapter 3 – The basic processes behind the operation of a typical solar cell are explained, the equivalent circuit and the solar cell's parameters are described, and external factors that affect the performance of the cell are discussed. Emphasis is given to the impact the temperature will have on all the processes and factors discussed above;
- Chapter 4 – Various computational simulations are made in order to better understand the effect the temperature will have on solar cells;
- Chapter 5 – Cooling methods are presented, and its advantages and drawbacks are discussed;
- Chapter 6 – Conclusions about the work are done. Recommendations and future work are proposed.

2. State of the Art

In 1839, French physicist Edmond Becquerel discovered the photovoltaic effect, showing that current and voltage were generated when a platinum electrode was illuminated. In 1883, Charles Fritts, using selenium, created the first solar cell, which had an efficiency of less than 1%. In 1954, Bell Labs announced the invention of the first practical silicon solar cell, and by the end of that decade Hoffman Electronics were developing commercial solar cells that could achieve a 10 % efficiency. During the 1960s and 1970s, solar cells were used to power several satellites and space stations, and by the late 70s they were being used by the general population. It becomes important to understand the way temperature affects the different types of solar cells.

2.1 Impact of Temperature on Solar Cells

While it is common knowledge that an increase in temperature negatively affects the output power and efficiency of solar cells, the impact of temperature on the different types of solar cells is not uniform, both in how it will affect the overall performance of the cell, but also how it will impact specific cell's parameters. Because of this, a review of the literature on the subject has been done, which follows.

2.1.1 Monocrystalline Silicon Solar Cell

Monocrystalline silicon (mono-Si) cells belong to the first generation of solar cells and are the oldest cells currently in the market. A review of the literature [2] finds that, for temperatures higher than 25 ºC, there will be a decrease in open circuit voltage, maximum power, fill factor and efficiency of the cell. There will also be a decrease in the band gap with an increase in temperature which will cause a slight increase in the short circuit current. The temperature coefficient for the P_{MP}, V_{OC} and FF will, therefore, all be negative and the coefficient for the I_{SC} will be positive. Figure 2.1 shows a typical current-voltage and a power-voltage curve for a monocrystalline silicon cell for several different temperatures, for a fixed solar irradiance.

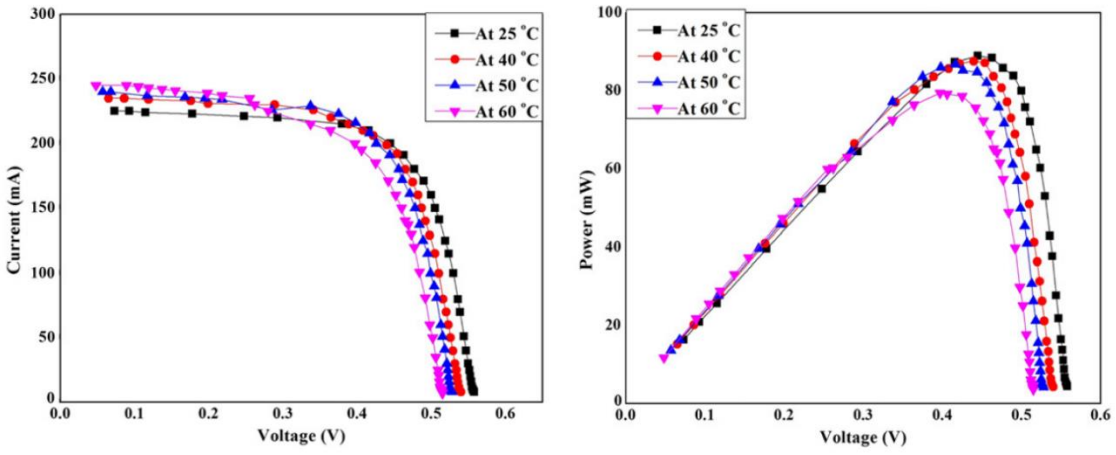

Figure 2.1 Current-voltage (left) and power-voltage (right) curves for a monocrystalline silicon cell for several different temperatures, for a fixed solar irradiance [2]

2.1.2 Polycrystalline Silicon Solar Cell

Polycrystalline silicon cells also belong to the first generation of solar cells and have recently surpassed their monocrystalline counterparts as the most sold cells in the market, despite being less efficient. The overall impact of the temperature on the solar cell's parameters is almost identical to the monocrystalline cells. However, polycrystalline solar cells have a lower heat tolerance than monocrystalline solar cells, so they tend to perform worse in warm weather, although the differences are relatively minor.

2.1.3 Amorphous Thin-Film Silicon Solar Cell

Amorphous silicon (a-Si) solar cells belong to the second generation of solar cells and are generally thought of as being very environment-friendly despite not being very efficient. They are made by depositing several thin layers of non-crystalline silicon onto a substrate. Unlike crystalline solar cells, amorphous silicon solar cells cannot be characterized by temperatures coefficients since the temperature dependence is typically non-linear and, in fact, some amorphous solar cells may even have an increase in efficiency for a certain range of temperatures higher than 25 ºC [3]. They tend to have better performances at high temperatures than crystalline solar cells [4] and, unlike those solar cells, the fill factor and short circuit current show significant increases with an increase in temperature. Amorphous cells tend to have relatively little temperature dependence once they are operating in an equilibrated state, however they will have a strong temperature dependence if the photovoltaic system experienced a sudden increase in temperature. For this latter case, some of the factors that affect the output power, and subsequently the efficiency of the solar cell, are the thickness and defect concentration of the i-layer and the device configuration. Figure 2.2 shows the normalized conversion efficiency of amorphous silicon solar cells, in comparison with other kinds of cells, where it is possible to observe the uneven effect the temperature may have on the cells.

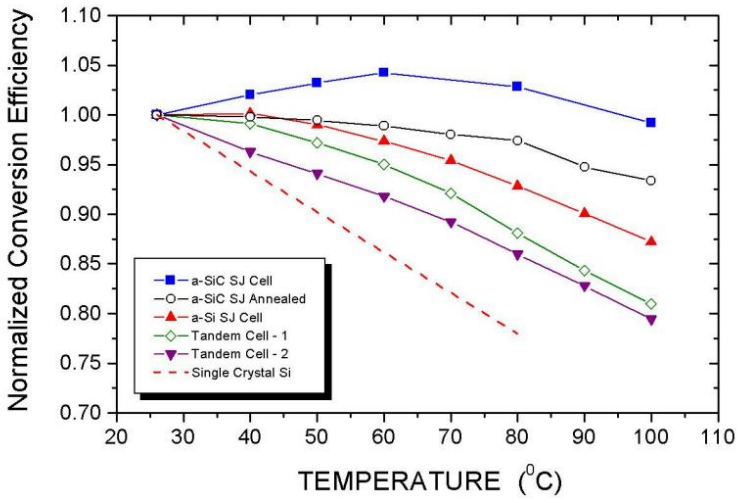

Figure 2.2 The normalized conversion efficiency of amorphous silicon solar cells and other types of cells as a function of temperature [3]

2.1.4 Multi-junction Solar Cell

Multi-junction (MJ) solar cells are cells with more than one p/n junction, each made of a different semiconductor material. By using different layers of semiconductor material, the MJ solar cells are capable of absorbing different wavelengths of sunlight. Recently, there has been great interest in these types of cells, since they can, theoretically, reach much higher efficiencies than single-junction cells, however high production costs means that they still are not in wide use by the general population. Most of the MJ solar cells produced use 3 layers of semiconductors. Usually, for the top layer of the cell, Indium gallium phosphide (InGaP) is used. For the middle layer, the semiconductor used is either gallium arsenide (GaAs) or indium gallium arsenide (InGaAs), while Germanium (Ge) is used in the bottom layer. When it comes to the short circuit current, the top layer of the cell will have a positive I_{SC} temperature coefficient, however this may or may not be the case for the remaining two layers of the cell. Since the middle and bottom layers will only capture part of the spectrum of sunlight, their I_{SC} temperature coefficients can be either positive or negative. The I_{SC} of the multi-junction cell will be limited by the lowest I_{SC} of the sub-cells, so with an increase in temperature the I_{SC} may either decrease or increase depending on semiconductor material used for the layers or the range of temperatures tested [5]. The open circuit voltage of the MJ cell will be the sum of the V_{OC} of the sub-cells. For all of the semiconductors used in the MJ cell, an increase in temperature will cause a decrease in the values of the V_{OC} [6], so therefore the overall temperature coefficient of the whole cell will be negative. With an increase in temperature there will also be a decrease in the fill factor and maximum power of the cell as well as an increase in the series resistance and a decrease in the shunt resistance [7]. Overall, MJ cells tend to have lower temperature coefficients than single-junction cells, meaning that they are less negatively affected by the temperature.

2.1.5 CIGS Solar Cell

Copper Indium Gallium Selenide (or CIGS) solar cells are another type of thin film solar cell that typically have good efficiencies and low costs of production, although there are concerns about the low availability of indium (In) and gallium (Ga). The semiconductor material has a chemical formula of $CuIn_xGa_{1-x}Se_2$ where the value of x can vary from 1 (pure copper indium selenide) to 0 (pure copper gallium selenide). A review of the literature [8] shows that an increase in the temperature of the CIGS solar cell will result in a slight decrease in the short circuit current, fill factor and quantum efficiency and a significant decrease in open circuit voltage accompanied by a decrease in the output power and efficiency. A CIGS solar cell is usually made up of a glass layer which is used as a substrate, a molybdenum (Mo) layer which serves as the back contact, the CIGS layer, the absorber, a cadmium sulfide (CdS) layer which is used as buffer and, finally, an intrinsic zinc oxide layer (i-ZnO). On top of all that, a luminescent down shifting (LDS) layer may also be placed on top of the photovoltaic material, which will enhance the performance of the solar cell both for normal and high temperatures conditions. Figure 2.3 shows the typical structure of a CIGS cell, both with and without a luminescent down shifting layer.

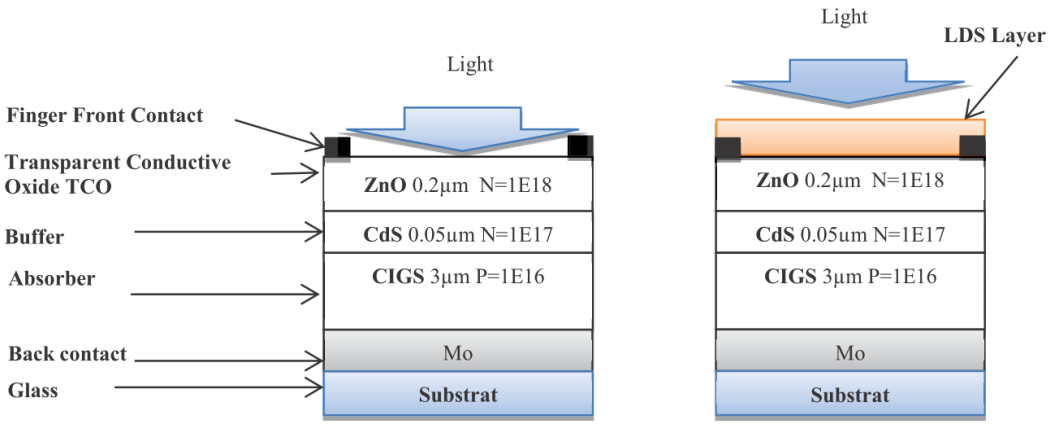

Figure 2.3 Structure of a CIGS solar cell, without a LDS layer (left) and with a LDS layer (right) [8]

2.1.6 CdTe Solar Cell

Cadmium telluride (CdTe) solar cells are thin-films solar cells that have lower costs than cells made of crystalline silicon, and that currently can reach an efficiency of about 22%. An increase in the temperature of a CdTe cell causes a slight increase in the short circuit current and a decrease in the open circuit voltage, fill factor, maximum power, and efficiency. For CdTe solar cells, the temperature coefficient for the V_{OC} is extremely similar to that of silicon-based cells, [6] however the overall efficiency coefficient is less pronounced, meaning that CdTe solar cells are not as affected by an increase in temperature as either monocrystalline or polycrystalline solar cells.

2.1.7 Organic Solar Cell

Organic solar cells belong to the third generation of solar cells and possess several advantages relative to silicon-based cells such as flexibility, low costs of production and a less adverse environmental impact, although they also have a considerably lower efficiency. For organic solar cells, the open circuit voltage decreases almost linearly with the temperature while the short circuit current will increase slightly with it until it reaches a maximum value of saturation and will subsequently decrease [9]. The behavior of the I_{SC} can perhaps be best explained by the changes in the charges carriers mobilities with the temperature. Unlike most types of solar cells, in organic cells the efficiency will actually increase with the temperature up until about 47 ºC, after which it will decrease [10]. Figure 2.4 shows the efficiency of an organic solar cell in function of the temperature, for several different irradiances. The fill factor behaves in a similar fashion to the efficiency.

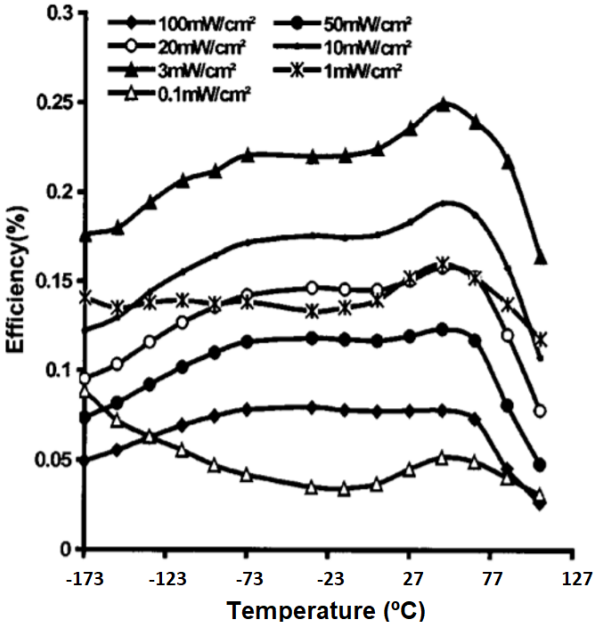

Figure 2.4 Efficiencies of an organic solar cell in function of the temperature, for various irradiances (adapted from [10])

2.1.8 Perovskite Solar Cell

Perovskite solar cells (PSCs) also belong to the third generation of solar cells and have recently attracted attention due to the technological advancements that have been made, in the past 10 years, in increasing their efficiency from 4% to about 30%. A PSC is a type of solar cell which includes a perovskite structured compound. Methylammonium lead halide (or $CH_3NH_3PbX_3$, where *X* = *I*, *Br* or *Cl*) is the most commonly used perovskite material.

Perovskite solar cells based on $CH_3NH_3PbI_3$ have been found to exhibit hysteresis in the I-V characteristics, meaning that the parameters and efficiency of the solar cell will be different depending if a forward scan (short circuit to open circuit) or a reverse scan (open circuit to short circuit) occurred. For perovskite solar cells, the unit cell volume calculated from the lattice parameters depends linearly on temperature and it has been shown that around 55 ºC the crystal structure $CH_3NH_3PbI_3$ changes from a tetragonal to a cubic phase. An analysis of the photovoltaic parameters in relation with the temperature, shows that hysteresis is observed at the temperature range of -20 ºC to +55 ºC, with a particular mismatch for the values of V_{OC} and FF. For both parameters, a reverse scan results in higher values and consequently the efficiency will be higher if a reverse scan occurred than it would be for a forward scan. The efficiency seems to reach its maximum value at about 30 ºC and drops at around 55 ºC as a result of the aforementioned phase transition of perovskite from tetragonal to cubic [11]. Figure 2.5 shows the efficiency of the perovskite cell in function of the temperature when a forward or a reverse scan is applied.

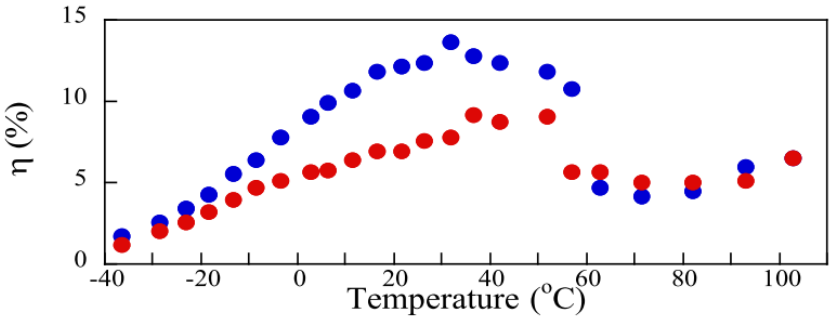

Figure 2.5 Efficiencies of a Perovskite solar cell in function of the temperature for a forward scan (red dots) and a reverse scan (blue dots) [11]

2.1.9 Quantum Dot Solar Cell

Quantum dot solar cells (QDSCs) are solar cells that use quantum dots as the absorbing photovoltaic material. Quantum dots are semiconducting particles, that have band gaps that are tunable across a wide range of energy levels. The tuning of the band gap makes quantum dot cells attractive since they can absorb different parts of the solar spectrum. Lead sulfide quantum dots (PbS QDs) have band gaps that can be tuned into infrared frequencies, making for a broad absorption profile. PbS QDs solar cells experience a decrease in the open circuit voltage, fill factor and efficiency, with an increase in the temperature. The short circuit current and the diode ideality factor, on the other hand, do not seem to be affected by the temperature [12]. In the case of a heterojunction quantum dot solar cell, where titanium dioxide (TIO_2) is used as the compact layer and PbS QD as the absorbing layer, there was a decrease in the I_{SC}, V_{OC}, and efficiency, with an increase in the temperature. There will also be a decrease in the value of the shunt resistance, with an increase in the temperature, which will cause a decline in the value of the fill factor [13].

2.1.10 CZTS Solar Cell

Copper zinc tin sulfide (CZTS) solar cells are thin films solar cells that have recently achieved efficiencies of about 12.6%. Compared with other thin-film solar cells, they have several advantages, such as lower costs of production and a less severe impact on the environment, although their efficiency is still lower than both CIGS and CdTe solar cells. A study [14], showed that for an increase in temperature from 26.85 ºC to 86.85 ºC of a CZTS cell, there was a linear decrease in the open circuit voltage and efficiency and a slight increase in the fill factor and short circuit current. Compared with CIGS cells, CZTS solar cells tend to have better behavior at high temperatures as their normalized output power (and therefore their conversion efficiency) is higher than in CIGS cells. Figure 2.6 shows the normalized conversion efficiency of both a CIGS and CZTS cell in function of the temperature.

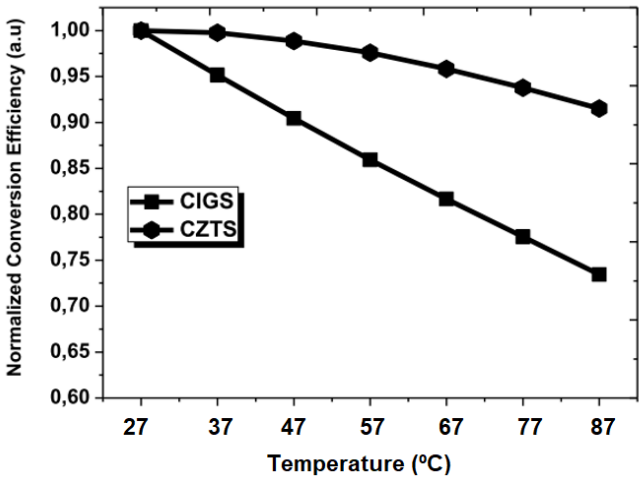

Figure 2.6 Normalized conversion efficiency of a CIGS and CZTS cell in function of the temperature (adapted from [14])

2.1.11 Gallium Arsenide Thin-Film Solar Cell

Gallium arsenide (GaAs) solar cells are another type of thin-film cells that can currently reach the highest efficiency of any single-junction solar cell. GaAs solar cells typically operate at a lower operating temperature than monocrystalline silicon cells, which is likely due to the higher band gap of GaAs and the high quality of the absorbing material [15]. With an increase in temperature, the short circuit current of the GaAs cell will increase, the open circuit voltage will decrease, and the fill factor will be almost entirely independent of the temperature of the cell. When it comes to the I_{SC}, its temperature coefficient will be more pronounced than in monocrystalline silicon cells, meaning that the I_{SC} will grow more with the increase in the temperature of the cell. This will happen because the band gap of the GaAs is larger and will shift more with the temperature than the band gap of the silicon. For the V_{OC}, it will not decrease, with the increase in temperature of the module, as much as the mono-Si cell, with the temperature coefficient being less than half it usually is in mono-Si cells. Because of the way the I_{SC} and V_{OC} change with the temperature, the maximum power will only slightly decrease with the temperature. A comparison between the normalized maximum power of the GaAs and mono-Si cell in function of the temperature can be seen in Figure 2.7.

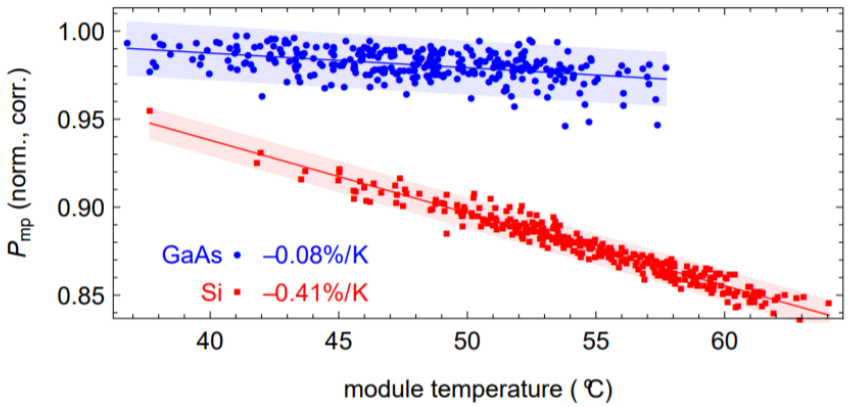

Figure 2.7 Normalized maximum power of a mono-Si and GaAs cell in function of the temperature [15]

2.1.12 Dye-sensitized Solar Cell

Dye-sensitized solar cells (DSSCs) are another type of thin-film solar cell who currently cannot reach the efficiencies of their thin-film cells counterparts or of silicon based cells, although they still possess several advantages such as a low cost of the materials, low toxicity and easy manufacturing. Unlike most types of cells, in DSSCs the recombination process in the active layer of the cell is roughly the same up until the temperatures of 40 ºC [16]. This in effect, means that the efficiency of the DSSC will only start to decrease when the cell will reach this temperature. Up until the temperature of 40 ºC, there will be a decrease in the value of the total series resistance which will cause an increase in the value of the fill factor which, in turn, will have a positive effect on the efficiency. The open circuit voltage will decrease with the temperature, having a more pronounced decay for temperatures higher than 40 ºC, since, from that point on, the recombination will increase. The short circuit current seems to remain the same for all temperatures [16].

3. Theoretical Framework

Having already previously established the effect that the temperature will have on different types of solar cells, in this chapter, a study has been conducted to understand the reasons why the temperature will have such an effect on the behavior and performance of a solar cell. The basic operation of a solar cell is described and the way the temperature influences said operation is explained, as is the temperature dependence of the cell's parameters. External factors that affect the temperature of the cell are also described.

3.1 Solar Cell Operation

When a solar cell is subjected to sunlight, photons will hit its surface. These photons may be either reflected off the surface, pass through it, or be absorbed by the semiconducting materials. This latter case will happen if the photon energy matches or is higher than the semiconductor band gap value and will subsequently cause the electrons (which had previously been held in place by the covalent bond between atoms) to gain energy from the photon and move from the valence band into the conduction band where they are free to move around the semiconductor and participate in the conduction process. The electron excitation leaves an empty space in the valence band which will be replaced by another electron which will subsequently leave another empty space. This continual movement of an empty space in the valence band is called a "hole" which can be described as being similar to an electron, but with a positive charge. Both the electrons and the holes are charge carriers and both participate in the conduction process. This generation of charge carriers will consequently generate a current that runs through the cell [17].

The recombination process is essentially the opposite of generation. Any electron that was excited into the conduction band, will eventually lose its energy and stabilize back to the valence band. In doing so, it will replace the hole that was present in the valence band. The amount of time a charge carrier can spend in an excited state before it recombines is called the *minority carrier lifetime*. The lifetime of the carriers is an indicator of the efficiency of the solar cell, and is dependent on the semiconductor material, so it is an important consideration when choosing the semiconductor. The carrier recombination lowers both the current and the voltage produced by the cell, so in order to maximize the efficiency of the solar cell, the generation of electron-holes should be maximized, and the recombination process should be minimized [17].

The band gap, the number of electrons or holes available for conduction, and the generation and recombination rate of the charge carriers are all important parameters of the semiconductor. They all play a significant part in the solar cell operation, so it becomes important to understand how these parameters can change in order to better improve the cell's performance.

The generation of charge carriers by itself, is not enough for electrical power generation. For this to happen, a voltage must also be generated. Most solar cells can be characterized as

essentially a large area p/n junction. A p/n junction consists of a n-type and p-type semiconductor material in contact with one another. Since the n-type side of the junction has a high electron concentration, and the p-type side has a high hole concentration, there will be a diffusion of electrons and holes into the p-type and n-type areas of the semiconductor, respectively. With this diffusion, positive ion cores will be exposed in the n-type side and negative ion cores will be exposed in the p-type side. An electric field, *E,* will form between the ion cores creating a depletion region which is mostly free of charge carriers. Due to the presence of the electric field, the built-in voltage will be created, which is a significant factor both in the p/n junction and in the operation of the solar cell. The voltage that forms across the solar cell, along with the current generated, means that the cell is capable of power generation which can be used to feed an external load [17]. The generation of the current and the voltage in a solar cell is known as the photovoltaic effect, which is shown in Figure 3.1.

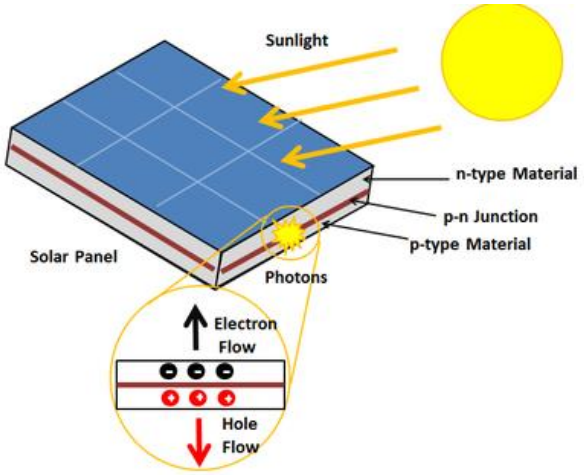

Figure 3.1 Diagram showcasing the photovoltaic effect [18]

Unfortunately, not all photons absorbed by the solar cell will result in the conversion of light into electricity. Photons, with more energy than the semiconductor band gap, which will be absorbed by the cell, will dissipate the difference of the energy in the production of heat (via lattice vibrations called phonons). The generation of heat will not be used into usable electrical energy, instead it will result in an increase in the cell's temperature which will have an impact on all the solar cell's processes like the generation and recombination, as well as on the proprieties of the semiconductor such as the band gap and the refractive index.

The electron carrier concentration, n, is the number of electrons per unit volume in the conduction band, and the hole carrier concentration, p, is the number of holes per unit volume in the valence band. In a semiconductor, the electron and hole carrier concentrations may not be necessarily the same, so the more abundant charge carriers are called the majority carriers, and the less abundant ones are called the minority carriers. At an equilibrium, when the generation and recombination are occurring at equal rates, the product of the majority and minority carrier concentrations is a constant, shown in the following expression:

$$n_0 p_0 = {n_i}^2 \tag{3-1}$$

where n_i is the intrinsic carrier concentration. If there is an excess of charge carriers then:

$$np > {n_i}^2 \tag{3-2}$$

at which point the recombination rate will become larger than the generation rate and the system will revert back to an equilibrium point. Similarly, if there is a shortage of charge carriers then:

$$np < {n_i}^2 \tag{3-3}$$

In this case the generation rate will become larger than the recombination rate, and the system will, once again, revert back to equilibrium.

The intrinsic carrier concentration is an important parameter which is linked to the solar cell's efficiency. It depends not only on the band gap, but also on the temperature. An increase in temperature makes it more likely that an electron will be excited into the conduction band, which causes an increase in the intrinsic carrier concentration. The intrinsic carrier concentration can be expressed in the following way:

$${n_i}^2(T) = N_C N_V e^{-E_g/kT} \tag{3-4}$$

where N_C and N_V are the effective density of states in the conduction and valence band respectively, T is the temperature expressed in Kelvin, k is the Boltzmann constant and E_g is the bandgap of the semiconductor. Both the effective density of states in the conduction and the valence band are dependent on the temperature of the semiconductor material and can be computed in the following way:

$$N_C\,(T) = 2\left(\frac{2\pi m_e^* kT}{h^2}\right)^{3/2} \tag{3-5}$$

$$N_V\,(T) = 2\left(\frac{2\pi m_h^* kT}{h^2}\right)^{3/2} \tag{3-6}$$

where the m_e^* and the m_h^* are the effective mass of the electron and hole respectively, which are dependent on the material of the semiconductor, and h is the Plank's constant. In reality, the effective mass of the electron and the hole are also temperature dependent, this being the result of changes in the electron-phonon interaction energies, but for simplicity sakes and because this temperature dependence does not greatly affect the intrinsic carrier concentration, the effect is not considered here [19]. Combining expression (3-4) with the expressions for the effective density of states, the expression for the intrinsic carrier concentration can be further developed:

$${n_i}^2(T) = 4\left(\frac{2\pi kT}{h^2}\right)^3 {m_e^*}^{3/2} {m_h^*}^{3/2} e^{-E_g/kT} \tag{3-7}$$

With the increase in the carrier concentration, there will be an increase in the internal carrier recombination rates which will negatively impact the performance of the cell. Also, with an increase in the temperature of the cell, the atoms and the electrons will vibrate faster and therefore the build-in voltage will be reduced.

3.2 Equivalent Circuit of Solar Cell

A solar cell may be modeled as a current source in parallel with a diode, along with a series and a shunt resistance, shown in Figure 3.2:

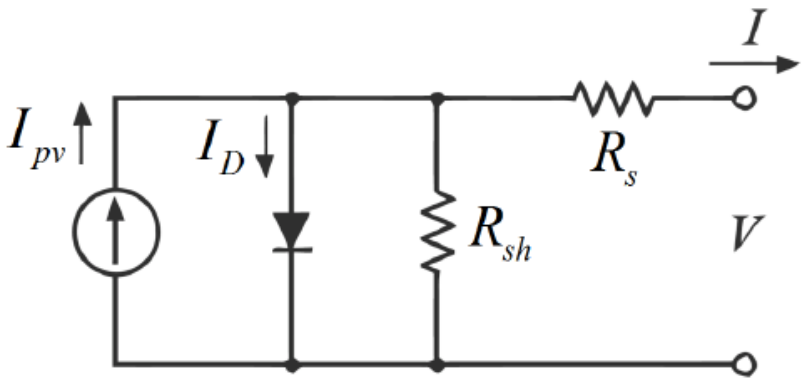

Figure 3.2 Equivalent Circuit of a Solar Cell [20]

where I_{pv} represents the light generated current, I_D the voltage-dependent current lost to recombination, and R_S and R_{SH} parasitic resistances which are added to the model because the solar cell is not ideal.

Making use of Kirchhoff's circuit laws, an expression for the characteristic equation of the solar cell can be derived, shown in the following expression:

$$I = I_{pv} - I_D - \frac{V + IR_S}{R_{sh}} \tag{3-8}$$

By the Shockley ideal diode equation, the expression for the I_D can be further developed in the following way:

$$I_D = I_s(e^{\frac{V_D}{nV_T}} - 1) \tag{3-9}$$

In the previous equation I_s represents the reverse saturation current, V_D the voltage across the diode, n the diode ideality factor and V_T the thermal voltage. The diode ideality factor is a dimensionless fitting parameter that measures how closely the diode's behavior matches the ideal diode equation. If the diode exhibits ideal behavior then $n = 1$, but usually its value is between 1 and 2. The expression for V_T can be further developed in the following way:

$$V_T = \frac{kT}{q} \tag{3-10}$$

where T is the temperature in Kelvin, k is the Boltzmann's constant which is approximately 1.38×10^{-23} J/K and q is the elementary charge which equals 1.6×10^{-19} C. At T = 25 ºC, $V_T \approx 0.0259\,V$. The characteristic equation of the solar cell can thus be further developed:

$$I = I_{pv} - I_s(e^{\frac{V+IR_S}{n\frac{kT}{q}}} - 1) - \frac{V + IR_S}{R_{SH}} \quad (3\text{-}11)$$

Based on the previous expression, the solar cell's current-voltage (I-V) characteristic curve can be traced, which essentially summarizes the relationship between the current and voltage of the cell. When the solar cell is open circuited the current will be at its minimum (zero) and the voltage across the cell is at its maximum which is designated as the open circuit voltage or V_{OC}. Similarly, when the cell is operated at short circuit, the voltage across the cell will reach its minimum (zero) and the current will reach its maximum which is designated as the short circuit current or I_{SC}. The power-voltage (P-V) curve can also be traced based on the I-V curve. An example of a typical I-V and P-V curve is shown in Figure 3.3.

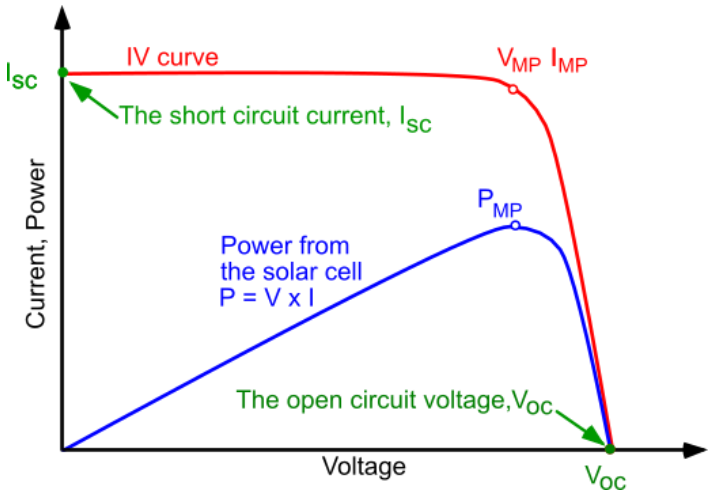

Figure 3.3 A typical I-V and P-V curve of a solar cell showcasing the performance parameters of the cell [21]

The power of the solar cell can be obtained by multiplying the current by the voltage. The point at which the solar cell generates the maximum power is known as the Maximum Power Point, or MPP, which is the ideal point of operation of the cell. The power at the MPP can be expressed as a function of the voltage and current observed at said point.

$$P_{MP} = V_{MP}.I_{MP} \quad (3\text{-}12)$$

The fill factor, FF, is a measure of the quality of the solar cell. It is defined as the ratio between the maximum power of the cell and the product of the V_{OC} and the I_{SC}.

$$FF = \frac{V_{MP}.I_{MP}}{V_{OC}.I_{SC}} \quad (3\text{-}13)$$

The solar cell efficiency, η, refers to the portion of energy in the form of sunlight that can be converted into electricity by the cell. It can be expressed as the ratio between the maximum power delivered by the cell and the incident power which is the area of the cell multiplied by the solar irradiance.

$$\eta = \frac{P_{MAX}}{A_{Cell}.G} \tag{3-14}$$

All the parameters of the characteristic equation of the solar cell are, in some way or another, influenced by the temperature, although it is especially significant for the I_s and the exponential part of the equation. An increase in temperature results in the decrease of the magnitude of the exponential of the equation. The reverse saturation current, I_s, can be expressed by the following equation:

$$I_s = q.A.{n_i}^2\left(\frac{D_p}{N_d}\frac{F_n}{L_p} + \frac{D_n}{N_a}\frac{F_p}{L_n}\right) \tag{3-15}$$

where A is the area of the cell, D_p and D_n are the diffusion coefficients of the holes and electrons respectively, N_d and N_a are the donor and acceptor concentrations respectively, L_n and L_p are the diffusion lengths of electrons and holes respectively and F_n and F_p are the finite recombination velocities of the electrons and holes, respectively. The intrinsic carrier concentration is the parameter in the above equation most affected by the temperature, in a manner previously explained, so that the I_s increases exponentially with an increase in temperature. The I_s can be expressed as a function of the temperature of the cell using the following expression:

$$I_s = {I_s}^*\left(\frac{T}{T^*}\right)^3 e^{\frac{E_g}{n}\left(\frac{1}{{V_T}^*}-\frac{1}{V_T}\right)} \tag{3-16}$$

where ${I_s}^*$, T^*, ${V_T}^*$ and n are the values of those parameters measured under standard test conditions (STC) and E_g is the band gap energy measured in electron-volt. The increase in the reverse saturation current is what causes a decrease in V_{OC}. Expressing the equation for the characteristic equation of the solar cell in terms of the V_{OC} wields:

$$V_{OC} \approx \frac{kT}{q}\ln\left(\frac{I_{pv}}{I_s}\right) \tag{3-17}$$

As can be seen from the previous equation, the exponential increase in the I_s causes a decrease for the V_{OC} for high temperatures. Also affected, albeit slightly, is the I_{pv} which increases slightly with increasing temperature because of an increase in the number of thermally generated carriers in the cell, as has been discussed before.

The diode ideality factor's temperature dependence is not well established, although it is found that, often, it decreases with the temperature. Part of the reason why the behavior of the ideality factor with the temperature is not well defined, is because it is hard to separate the effect that the temperature will have on the ideality factor, with the changes the ideality factor will suffer due to the change in the other parameters with the temperature.

Likewise, when it comes to the parasitic resistances, the effect of the temperature is also hard to map. For the series resistance, one study suggests that, for silicon solar cells, using the one diode circuit model, there is a decrease in R_S with an increase in temperature, while the opposite is true for a two-diode model [22]. The increase in the series resistance with the temperature may be associated with the decreased mobility of the charge carriers that comes with an increase in temperature.

For silicon solar cells, an increase in the temperature, appears to cause a decrease in the value of the shunt resistance, which negatively impacts the performance of the solar cell [23]. This decrease may be caused by the increase in leakage current that is the result of the increase in the generation of charge carriers, caused by the temperature. It is also possible, that this effect could be overshadowed by the, previously mentioned, decrease mobility in the charge carriers, in which case the R_{SH} would increase with the temperature.

3.3 External Factors

Since the exposure of solar cells to sunlight generates heat as well as electricity, their temperature will not be the same as the ambient temperature. It is however possible to express one in function of the other. One such expression follows:

$$T_{CELL} = T_{AMB} + \frac{G}{G_{NOCT}}(T_{CELL_{NOCT}} - T_{AMB_{NOCT}}) \tag{3-18}$$

where T_{AMB} is the ambient temperature, G is the solar irradiance that hits the solar cell, G_{NOCT} is the solar irradiance under Nominal Operating Cell Temperature (NOCT) which equals 800 W/m^2, $T_{AMB_{NOCT}}$ which is the ambient temperature of the cell under NOCT conditions equaling 20 ºC and $T_{CELL_{NOCT}}$ is the cell temperature under NOCT conditions. The previous expression can thus be simplified in the following way:

$$T_{CELL} = T_{AMB} + \frac{G}{800}(T_{CELL_{NOCT}} - 20) \tag{3-19}$$

The previous equation does not take into account other important factors that affect the temperature of the solar cells such as the wind velocity, the wind azimuth angle and the tilt angle of the panel. With an increase in wind velocity comes a decrease in the temperature of the panel, which is due to the fact that there is an increment in heat losses which results in a decrease in the temperature and consequently an increase in the performance of the solar panel [24].

The wind azimuth angle is the direction from which the wind originates, and its effect on the temperature of the photovoltaic system is correlated with the tilt angle of the solar panel and the wind velocity. The optimum tilt angle of the panel is dependent on the latitude and longitude of the location where the photovoltaic system is installed, being lower for places at lower latitudes and higher for places at higher latitudes. An approximate optimal tilt angle of the panel in Lisbon during the winter would be 52° facing the south. For this case, an increase in the wind azimuth

angle would lead to an increase in the temperature of the panel. For the same location, if the wind azimuth angle is 0°, an increase in the tilt angle of the panel will lead to a decrease in the temperature of the photovoltaic system.

Solar irradiance is usually thought of as being independent of the temperature, but in fact both parameters are correlated. With an increase in irradiance comes an increase in heat generation and, thus an increase in the temperature of the cell. On the other hand, irradiance also contributes positively to the output power of the solar cell which tends to dominate over the negative effect caused by the increase in the temperature of the cell. Assuming the temperature of the cell is constant, it is common to express the short circuit current in function of the irradiance in the following way:

$$I_{SC}(G) = \frac{G}{G_{STC}} I_{SC\,STC} \tag{3-20}$$

where G is the solar irradiance, G_{STC} is the irradiance under standard test conditions (STC) which equals 1000 W/m^2 and $I_{SC\,STC}$ is the short circuit current under STC conditions. The open circuit voltage also varies with the irradiance, albeit in a less pronounced way. An example of how a typical I-V curve of a solar cell varies with the irradiance can be seen in Figure 3.4.

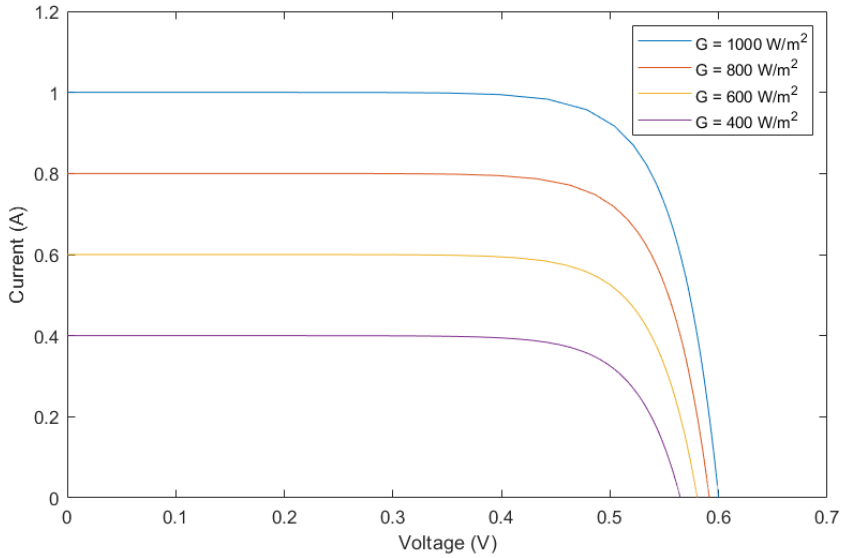

Figure 3.4 I-V curves of a solar cell for different solar irradiances

4. Computational Simulations

In this section, several computational simulations were conducted in order to better understand the impact the temperature will have on solar cells. Always using a finite element simulation software, the behavior of different types of solar cells with the temperature was simulated, and the temperature dependence of certain parameters, and the impact they will have on the solar cell, was studied. The computation simulations were done for both 1D and 2D models and comparisons were drawn.

4.1 1D Solar Cells

Using a finite element simulation software, 1D models of 4 different types of solar cells were created. Using the semiconductor module, the p/n junction is made by using an analytic doping model for uniform bulk n-doping, and a geometric doping model is used for the front surface p-doping. The front surface is defined as the point to the furthest left of the geometry of the cell. Two metal contacts are added to the model, with each of them being located at the extremities of the cell. These metal contacts serve to form an electric connection between the front and the back surface of the cell. One metal contact will be grounded, while the other one will have a voltage applied to it, which will make the production of electrical power possible. In all 4 cases, solar cells with a diameter of 150 µm were designed. For all simulations, for the solar spectrum an approximation of the AM1.5 Global spectrum was used. This spectrum was used because it provides a good representation of the irradiance a solar panel would receive in a clear day in the middle latitudes. The design of the 1D solar cell can be seen in Figure 4.1.

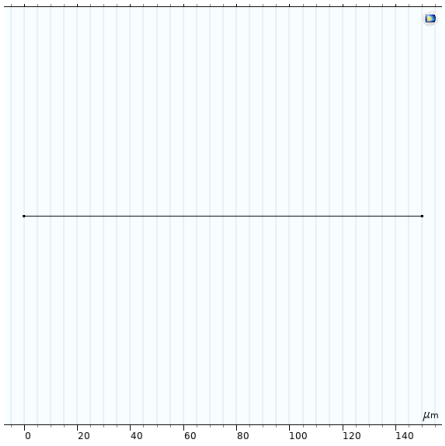

Figure 4.1 Geometry of the 1D Solar Cell

For each type of solar cell, relevant data about the material such as the band gap, the electron affinity, and the effective density of states was inputted into the model. Furthermore, in order to achieve a greater accuracy, the complex refractive index of each material was also added to the computations. The photogeneration rate of the charge carriers was computed through the following formula:

$$G(z) = \int_0^{\infty} \alpha(\lambda)\,(1 - R(\lambda))\phi(\lambda)e^{-\alpha(\lambda)z}d\lambda \quad (4\text{-}1)$$

where z is the depth into the device from the surface, λ the wavelength and $R(\lambda)$ is the reflection coefficient which is calculated from the following expression:

$$R(\lambda) = \frac{(n(\lambda) - 1)^2 + k(\lambda)^2}{(n(\lambda) + 1)^2 + k(\lambda)^2} \quad (4\text{-}2)$$

where $n(\lambda)$ and $k(\lambda)$ are the real and imaginary part of the complex refractive index of the material, respectively. $\alpha(\lambda)$ the absorption coefficient defined by:

$$\alpha(\lambda) = \frac{4\pi.k(\lambda)}{\lambda} \quad (4\text{-}3)$$

The photon generation rate, $\phi(\lambda)$, is the measured number of photons per area per time, defined by:

$$\phi(\lambda) = \frac{\lambda}{h.c}F(\lambda) \quad (4\text{-}4)$$

where $F(\lambda)$ is the spectral irradiance, h is the Plank's constant and c is the speed of light in vacuum. When it comes to the recombination, the Shockley-Read-Hall model was employed.

For all the simulations, whenever a temperature coefficient is mentioned it is always expressed in %/ºC to allow for an easier comparison between the different types of cells and different experiments. The temperature coefficient also always refers to the lowest temperature measured for any particular experiment. For instance, in the next simulation, the silicon open circuit voltage temperature coefficient indicates the decrease the that V_{OC} will suffer, with an increase in temperature, relating to the measure taken at 25 ºC.

4.1.1 Silicon Solar Cell

Firstly, a simulation of the effect of different temperatures on a silicon solar cell was made. Four different temperatures of the material were tested, the I-V and P-V curves were computed and can be seen in Figure 4.2. As can be seen in Table 1, the computational results are in accordance with the review of the literature that was conducted [2]. With an increase in the temperature there was a decrease in the open circuit voltage, maximum power, and fill factor. For the V_{OC} and the P_{MP} the temperature coefficients were, respectively, approximately -0.37 %/°C and -0.47 %/°C. With regards to the short circuit current, there was, as expected, a slight increase with the temperature, with a coefficient of about +0.005 %/°C, although the increase was less pronounced than is usual for silicon solar cells. In the case of the fill factor, there was an expected decrease with the temperature with a coefficient of about -0.11 %/°C.

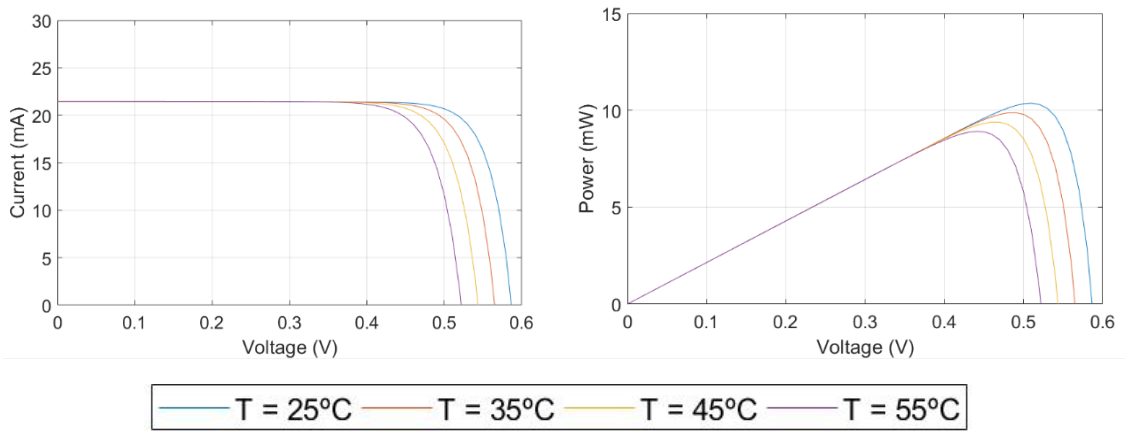

Figure 4.2 I-V and P-V curves for the 1D silicon solar cell for 4 different temperatures

Table 1 Solar cell parameters' data for the 1D silicon solar cell for 4 different temperatures

T[°C]	$I_{SC}\ [mA]$	$V_{OC}\ [V]$	$P_{MP}\ [mW]$	FF
25	21.44	0.588	10.39	0.824
35	21.45	0.566	9.90	0.815
45	21.46	0.544	9.41	0.806
55	21.47	0.523	8.93	0.795

4.1.2 CIGS Solar Cell

Figure 4.3 and Table 2 show the results of the simulation of a CIGS solar cell. Pure copper indium selenide (or $CuInSe_2$) was used as the semiconductor material of the cell, so more accurately, a simulation of a CIS cell was done. For the CIS solar cell, there was virtually no change in the I_{SC} with the variation in temperature. For the V_{OC} and the P_{MP}, there was a temperature coefficient of about -0.26 %/°C and -0.34 %/°C, respectively. The temperature coefficients show that in comparison with a silicon solar cell, the efficiency of the CIS cell is not as negatively affected by the temperature, with both the V_{OC} and the P_{MP} being less affected by an increase in the temperature. The fill factor had a coefficient of about -0.09 %/°C.

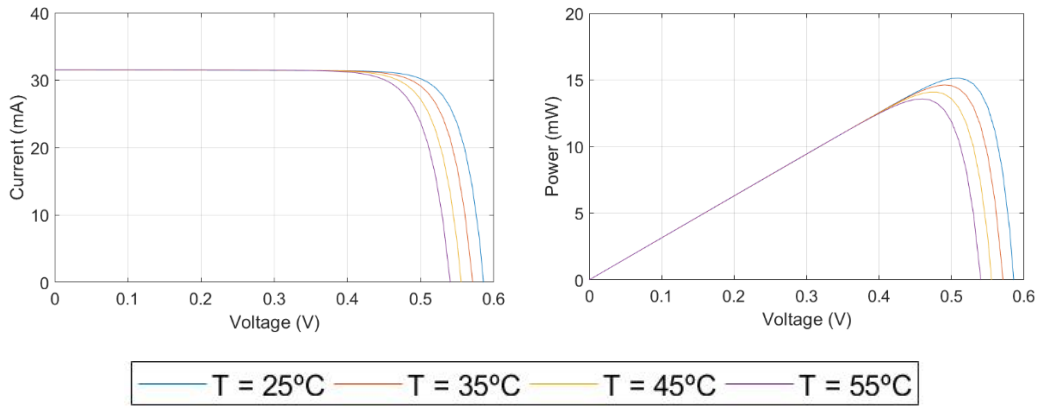

Figure 4.3 I-V and P-V curves for the 1D CIGS solar cell for 4 different temperatures

Table 2 Solar cell parameters' data for the 1D CIGS solar cell for 4 different temperatures

T[ºC]	I_{SC} $[mA]$	V_{OC} $[V]$	P_{MP} $[mW]$	FF
25	31.51	0.586	15.14	0.820
35	31.51	0.571	14.62	0.813
45	31.51	0.555	14.08	0.805
55	31.51	0.540	13.58	0.798

4.1.3 CdTe Solar Cell

A simulation of a Cadmium Telluride solar cell was next conducted, and the resulting I-V and P-V curves can be seen in Figure 4.4. As can be seen in Table 3, with an increase in the temperature of a CdTe solar cell, there was a slight increase in the I_{SC} and a decrease in the V_{OC}, P_{MP} and *FF*, which is all corroborated by the review of the literature that was done [6]. The V_{OC} and P_{MP} had a temperature coefficient of -0.18 %/°C and -0.23 %/°C, respectively. For the CdTe cell, it was found that, just like the literature indicated, the P_{MP} and consequently the efficiency is not as negatively affected by an increase in the temperature as is the case for silicon-based cells. However, the variation of the V_{OC} with the temperature was less pronounced than was expected, since the temperature coefficient of the V_{OC} was considerably smaller than in the silicon solar cell. The temperature coefficient of the fill factor was about -0.05 %/ºC, lower than both the silicon and the CIGS cell.

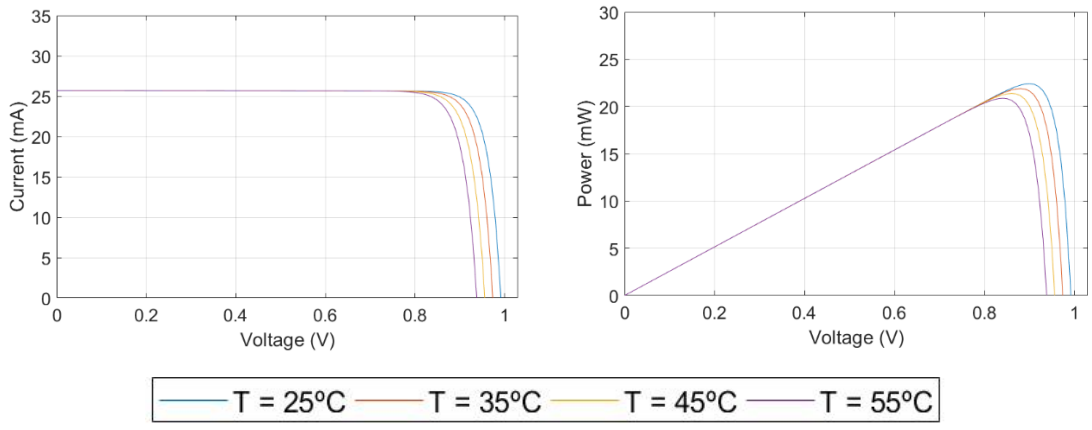

Figure 4.4 I-V and P-V curves for the 1D CdTe solar cell for 4 different temperatures

Table 3 Solar cell parameters' data for the 1D CdTe solar cell for 4 different temperatures

T[ºC]	I_{SC} $[mA]$	V_{OC} $[V]$	P_{MP} $[mW]$	FF
25	25.71	0.992	22.42	0.879
35	25.71	0.974	21.90	0.875
45	25.72	0.956	21.39	0.870
55	25.72	0.938	20.87	0.865

4.1.4 Perovskite Solar Cell

Figure 4.5 and Table 4 show the results of the simulation of the behavior of a perovskite solar cell, using methylammonium lead iodide ($CH_3NH_3PbI_3$) as the material of the semiconductor. For the perovskite solar cell, an increase in the temperature led to a decrease in the value of the open circuit voltage and maximum power, and a slight increase in the short circuit current. The open circuit voltage and maximum power had a temperature coefficient of -0.14 %/°C and -0.18 %/°C respectively, showing that the PSCs are, of all the cells simulated, the least negatively affected by the temperature. The FF had a temperature coefficient of -0.045 %/ºC.

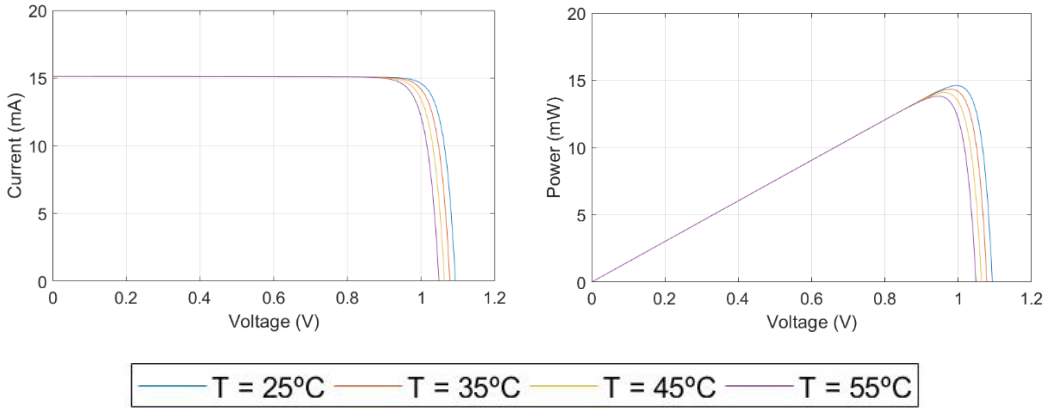

Figure 4.5 I-V and P-V curves for the 1D Perovskite solar cell for 4 different temperatures

Table 4 Solar cell parameters' data for the 1D Perovskite solar cell for 4 different temperatures

T[ºC]	I_{SC} $[mA]$	V_{OC} $[V]$	P_{MP} $[mW]$	FF
25	15.11	1.093	14.60	0.884
35	15.11	1.078	14.34	0.880
45	15.12	1.063	14.08	0.876
55	15.12	1.048	13.82	0.872

The normalized open circuit voltage and maximum power of all 4 solar cells can be seen in Figures 4.6 and 4.7, showcasing the different impact the temperature will have on the performance of the cells. The efficiency of the solar cells will decrease in much the same way as the maximum power, since neither the area of the cell nor the irradiance suffered any changes with the increase in temperature.

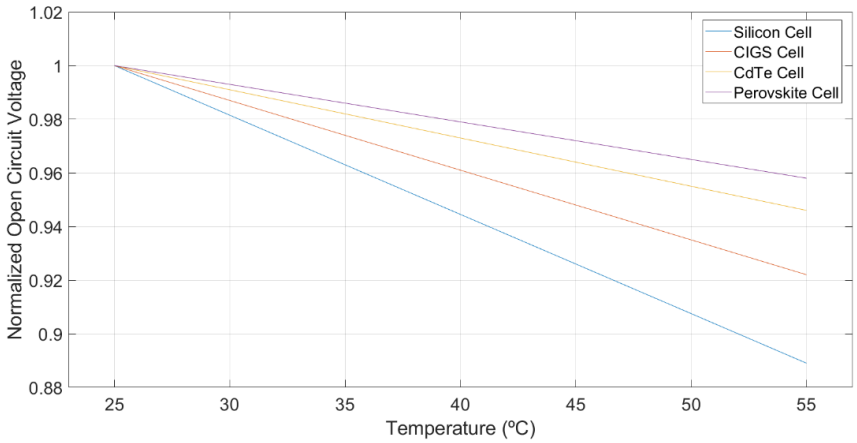

Figure 4.6 Normalized open circuit voltage as a function of the temperature for the 4 solar cells

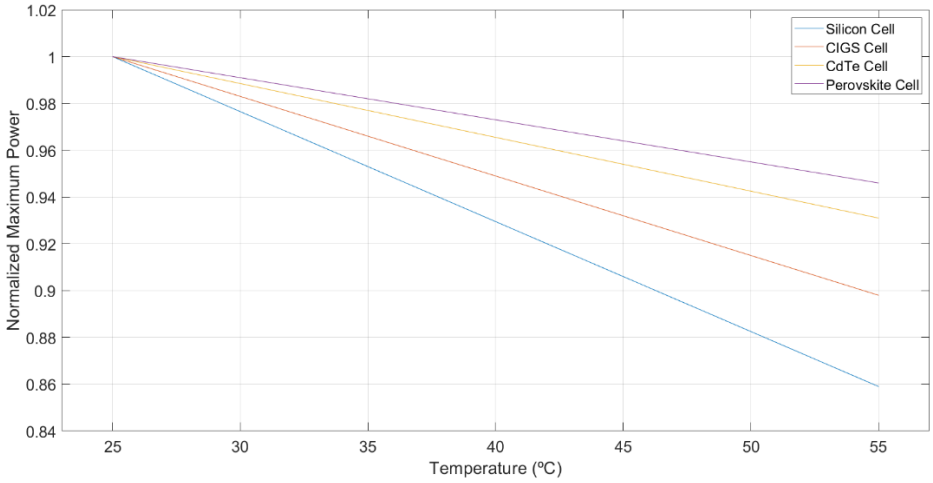

Figure 4.7 Normalized maximum power as a function of the temperature for the 4 solar cells

4.2 The Temperature Dependence of the Band Gap

The band gap of the semiconductor material is an important parameter in the performance of the solar cell. The band gap is the energy difference between the conduction and the valence band, so, in other words, it is the minimum energy necessary to excite the electron and have it participate in the conduction process. The semiconductor will not absorb photons with energy lower than the band gap, and if the band gap of the semiconductor is too low, most of the photons will have higher energies than is needed to excite the electrons. Because of this, the efficiency of the solar cell is directly related to the semiconductor band gap. The Shockley–Queisser limit (shown in Figure 4.8) expresses the maximum efficiency of a single-junction solar cell in function of the band gap of the semiconductor. For single-junction solar cells, and assuming typical sunlight conditions, their maximum theoretical efficiency is around 33.7%. For multi-junction solar cells, the maximum theoretical efficiency is considerably higher, being around 86%.

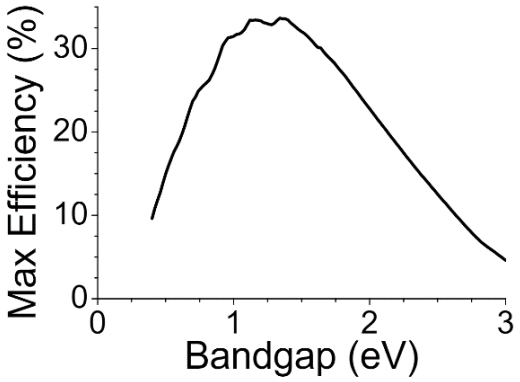

Figure 4.8 The Shockley–Queisser limit of a single junction solar cell

As was previously noted in section 3.1, the band gap of the semiconductor material is directly affected by the temperature. As the temperature increases, the amplitude of atomic vibrations increase, which will subsequently increase the interatomic spacing and cause the interatomic bonds to be weakened, which means that less energy is needed to excite an electron into the conduction band and therefore there will be a decrease in the semiconductor's band gap. The interaction between the phonons and the charge carriers will also contribute to the decrease in band gap with the temperature. The relationship between some semiconductor's band gap and its temperature can be approximated by the Varshni equation, shown in expression (4-5):

$$E_g(T) = E_g(0) - \frac{\alpha\, T^2}{T + \beta} \tag{4-5}$$

where α and β are, material-dependent, fitting parameters (which are expressed in eV/K and K respectively) and $E_g(0)$ is the bandgap observed at 0 K. An example of the numerical values of the parameters of expression 4-5 for 3 different semiconductors can be seen in Table 5.

Table 5 Fitting parameters of the Varshni equation for 3 different semiconductors

	Germanium	Silicon	Gallium arsenide
$E_g(0)\ [eV]$	0.744	1.166	1.519
$\alpha\ [eV/K]$	4.77×10^{-4}	4.73×10^{-4}	5.41×10^{-4}
$\beta[K]$	235	636	204

For the case of silicon, the variation of the band gap with the temperature can be seen in Figure 4.9.

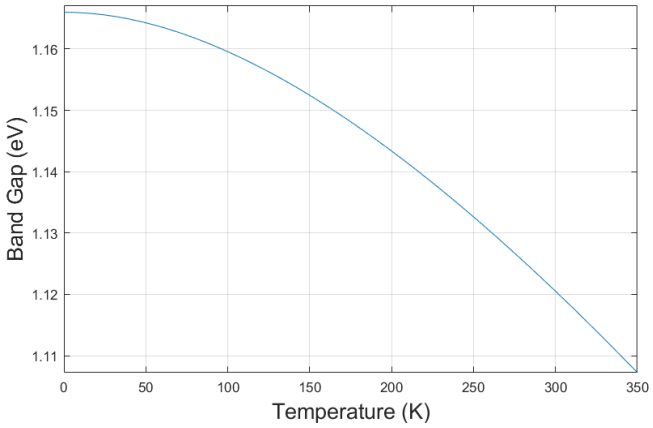

Figure 4.9 The variation of the silicon band gap with the temperature

As can be seen by the previous figure, the temperature dependence of the band gap for silicon solar cells operating under temperatures that could reasonably be reached by said cells, is not very strong. However, it is still important to know how the change in band gap of the semiconductor with the temperature affects the performance of the cell. Previously, when simulating the behavior of the one-dimensional silicon solar cell, the value of the band gap inputted into the model equaled 1.121 eV which is the value of the bang gap of silicon measured at about 25 ºC. Now, in order to study the impact the change in band gap with the temperature will have on the performance of the solar cell, the I-V and P-V curves of the cell were computed for different temperatures using both the fixed 1.121 eV value and the more accurate calculated temperature dependent value. Tables 6, 7, 8 and Figures 4.10, 4.11 and 4.12 show the results of the computations.

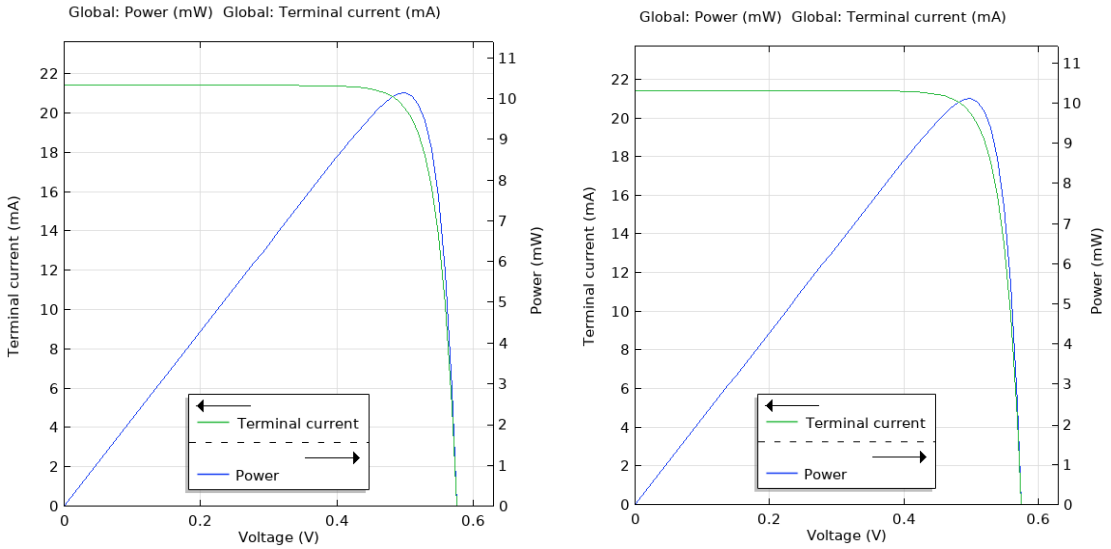

Figure 4.10 I-V and P-V curves for the 1D silicon solar cell measured at 30 ºC with a band gap of 1.121 eV (left) and 1.120 eV (right)

Table 6 Solar cell's parameters for the 1D silicon solar cell for 2 different band gaps measured at 30 ºC

$E_g(30)\ [eV]$	$I_{SC}\ [mA]$	$V_{OC}\ [V]$	$P_{MP}\ [mW]$	FF
1.121	21.44	0.577	10.15	0.820
1.120	21.44	0.576	10.12	0.819

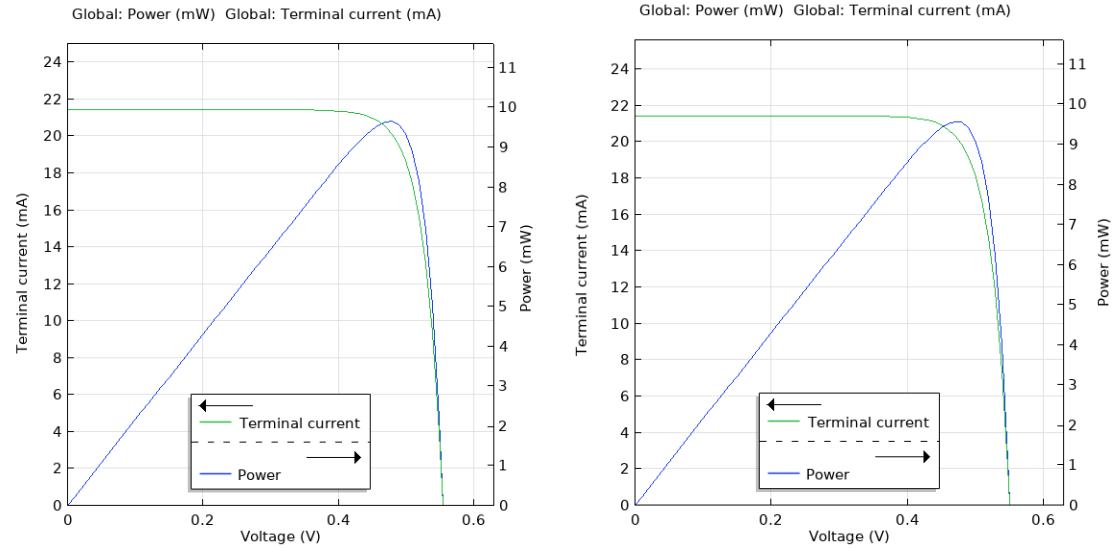

Figure 4.11 I-V and P-V curves for the 1D silicon solar cell measured at 40 ºC with a band gap of 1.121 eV (left) and 1.117 eV (right)

Table 7 Solar cell's parameters for the 1D silicon solar cell for 2 different band gaps measured at 40 ºC

$E_g(40)[eV]$	$I_{SC}\ [mA]$	$V_{OC}\ [V]$	$P_{MP}\ [mW]$	FF
1.121	21.46	0.555	9.66	0.811
1.117	21.46	0.551	9.58	0.810

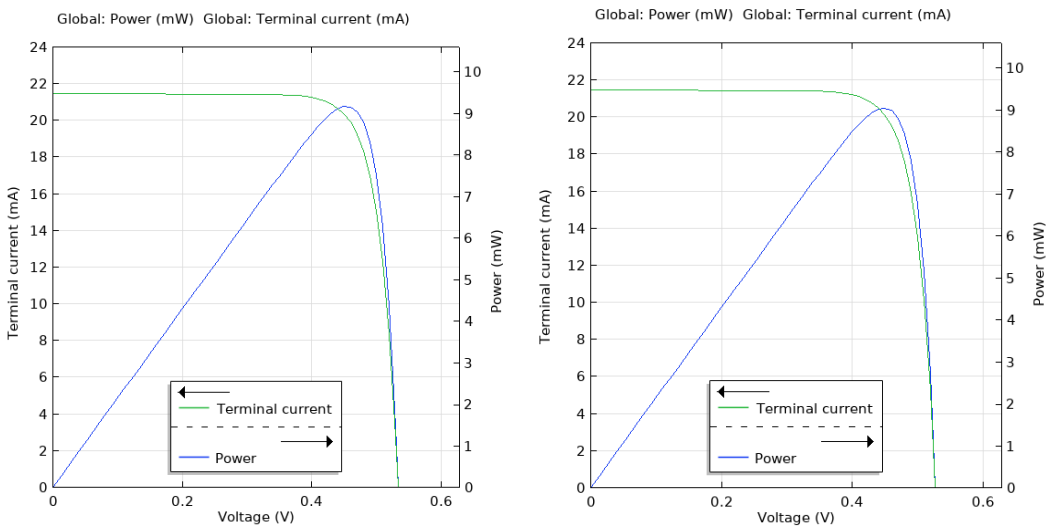

Figure 4.12 I-V and P-V curves for the 1D silicon solar cell measured at 50 ºC with a band gap of 1.121 eV (left) and 1.115 eV (right)

Table 8 Solar cell's parameters for the 1D silicon solar cell for 2 different band gaps measured at 50 ºC

$E_g(50)[eV]$	$I_{SC}\ [mA]$	$V_{OC}\ [V]$	$P_{MP}\ [mW]$	FF
1.121	21.47	0.533	9.17	0.801
1.115	21.47	0.528	9.06	0.799

As can be seen by Tables 6, 7 and 8, with a decrease in band gap comes a decrease in the open circuit voltage, maximum power, and overall performance of the cell. The short circuit current and fill factor, on the other hand, seem to be relatively unaffected. The decrease in open circuit voltage can be explained by the effect the band gap will have on the intrinsic carrier concentration. With a decrease in the band gap, the intrinsic carrier concentration will increase which can be seen in expression (3-7). As was explained in section 3.2, the increase in intrinsic carrier concentration will lead to an increase in the reverse saturation current which will cause a decrease in the open circuit voltage. The decrease in band gap does not have as large an impact on the intrinsic carrier concentration as the effective density of states, but with higher temperatures the effect will progressively increase. The relationship between the semiconductor band gap and the temperature can be better understood by the following expression which relates the band gap with the minimum value of the reverse saturation current density:

$$J_S = \frac{q}{k}\frac{15\sigma}{\pi^4}T^3\int_u^\infty \frac{x^2}{e^x - 1}dx \tag{4-6}$$

where q is the electronic charge, σ is the Stefan–Boltzmann constant and

$$u = \frac{E_g}{kT} \tag{4-7}$$

By using expression (4-6) and tracing the reverse saturation current density in function of the band gap, it becomes clear that with a decrease in band gap, the minimum value of J_S will

increase. The decrease in the open circuit voltage will subsequently cause a decrease in the value of the maximum power.

With the, temperature dependent, band gap taken into consideration, more accurate values of the temperature coefficients of the open circuit voltage and maximum power of the silicon solar cell can be computed. The V_{OC} has a temperature coefficient of about -0.41 %/ºC and the P_{MP} has a temperature coefficient of about -0.52 %/ºC.

For the short circuit current, the decrease in the band gap of the semiconductor with an increase in temperature should theoretically lead to an increase in the value of the I_{SC} since a larger part of the solar spectrum can be absorbed by the cell which will subsequently cause an increase in the current generated. In terms of the computational simulations, however, it appears that the decrease in band gap with the temperatures that are usually reached by the solar cells does not have a great effect on the I_{SC}.

4.3 The Temperature Dependence of the Refractive Index

The refractive index of a material is a dimensionless number that relates how fast lights travels through the material. It is defined as the ratio between the speed of light in vacuum and the phase velocity of light in the medium, which can be seen in the following expression.

$$n = \frac{c}{v} \tag{4-8}$$

When light travels through a medium at least some part of it will be attenuated, meaning that there will be a reduction in the intensity of light as it passes through a medium. Due to this, a complex refractive index can be defined, where this phenomenon is taken into account, by the introduction of an imaginary part to the refractive index, shown in the following expression.

$$\bar{n} = n + jk \tag{4-9}$$

In the previous expression, *n* is the refraction index and refers to the phase velocity of light in the material and the *k* is the extinction index. The extinction index is directly responsible for the absorption of light into the medium and it is correlated with the absorption coefficient as can be seen in expression (4-3).

Both the real and the imaginary parts of the complex refractive index are directly affected by the temperature of the material, photon energy and wavelength of the solar spectrum. For the case of silicon, a review of the literature was conducted in order to understand how the complex refractive index is affected by the temperature of the material. It was found that, for temperatures that solar cells can realistically be expected to reach, with an increase in the temperature there will be an increase in the refraction and extinction index, regardless of the wavelength of the solar spectrum [25] [26]. For all wavelengths above 450 nm and below 1100 nm, and for all temperatures above 298 K, the real part of the complex refractive index, *n*, can be expressed as

a function of both the wavelength of the radiation and the temperature [27]. The relationship between the real part of the complex refractive index and the temperature, shown in the following expression, shows how the refractive index is a linear function of temperature.

$$n(\lambda, T) = n_0(\lambda) + a_n(\lambda)(T - T_{0n}) \tag{4-10}$$

In the above expression, T_{0n} is the reference temperature which equals $25\,°C$, $n_0(\lambda)$ is the reference refractive index taken at $25\,°C$ and $a_n(\lambda)$ is a fitted polynomial function which is defined in the following way:

$$a_n(\lambda) = A(0) + A(1)\lambda + A(2)\lambda^2 + A(3)\lambda^3 + A(4)\lambda^4 + A(5)\lambda^5 + A(6)\lambda^6 + A(7)\lambda^7 \tag{4-11}$$

where the *A* coefficients are known, and λ is in nm. For the case of the extinction index, *k*, and for wavelengths of sunlight between 450 nm and 840 nm, its temperature dependence can be expressed as an exponential function, shown in the following expression [28]:

$$k(\lambda, T) = k_0(\lambda) e^{T/T_0(\lambda)} \tag{4-12}$$

where $k_0(\lambda)$ and $T_0(\lambda)$ are both fitted functions, shown in the following two expressions.

$$k_0(\lambda) = -0.0805 + e^{-3.1893 + \frac{7.946}{13.31 - \frac{1.537}{\lambda^2}}} \tag{4-13}$$

$$T_0(\lambda) = 369.9 - e^{-12.92 - \frac{6.83}{\lambda}} \tag{4-14}$$

In both previous expressions the λ is expressed in µm. For wavelengths between 840 nm and 1100 nm, an extrapolation of the values of the extinction index was made. When the I-V and P-V curves of the silicon solar cell were simulated in section 4.1, the complex refractive index remained the same for all the temperatures tested. In that case, the complex refractive index had been taken from a refractive index library and referred to silicon at 25 ºC. Now, in order to observe the effects of the, temperature-dependent, complex refractive index on the performance of the silicon solar cell, several tests were conducted on the one-dimensional cell. For three different temperatures, the temperature-dependent complex refractive index was calculated, and the I-V and P-V curves were computed with it taken into account. The resulting curves were then compared with they would be like if the model had taken the temperature independent complex refractive index (measured at 25 ºC) into consideration. Figures 4.13, 4.14 and 4.15 and Tables 9, 10 and 11 show how the complex refractive index affected the performance of the solar cell.

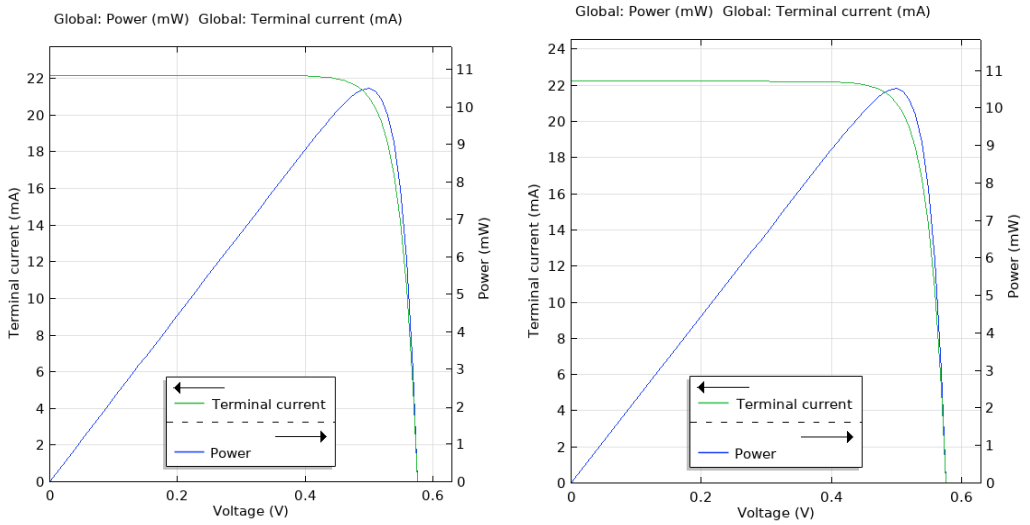

Figure 4.13 I-V and P-V curves for the 1D silicon solar cell measured at 30 ºC with the original complex refractive index (left) and adjusted complex refractive index (right)

Table 9 Solar cell's parameters for the 1D silicon solar cell for at 30 ºC with the original and adjusted complex refractive index

Refractive Index	$I_{SC}\ [mA]$	$V_{OC}\ [V]$	$P_{MP}\ [mW]$	FF
Original	22.21	0.577	10.50	0.819
Adjusted	22.25	0.577	10.53	0.820

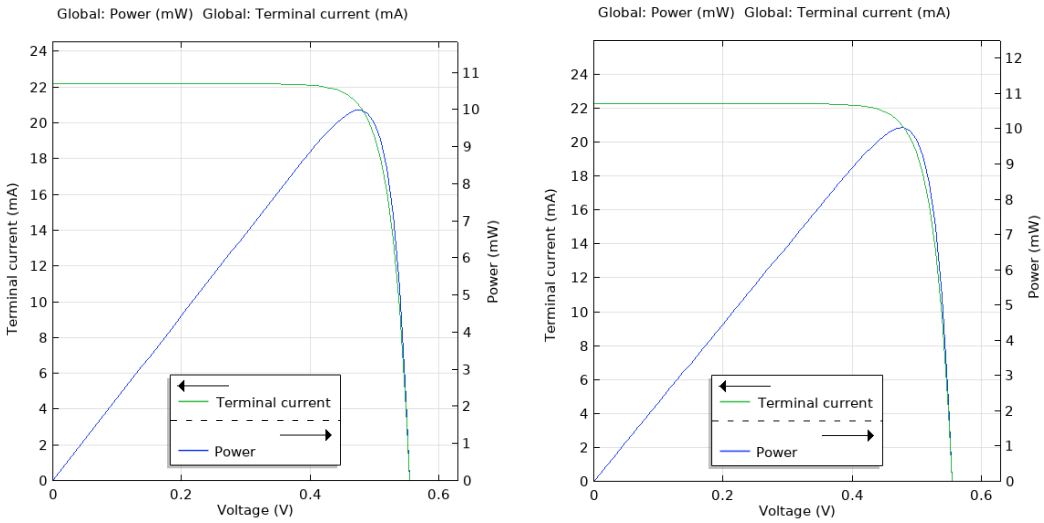

Figure 4.14 I-V and P-V curves for the 1D silicon solar cell measured at 40 ºC with the original complex refractive index (left) and adjusted complex refractive index (right)

Table 10 Solar cell's parameters for the 1D silicon solar cell for at 40 ºC with the original and adjusted complex refractive index

Refractive Index	$I_{SC}\ [mA]$	$V_{OC}\ [V]$	$P_{MP}\ [mW]$	FF
Original	22.22	0.555	10.00	0.811
Adjusted	22.31	0.555	10.04	0.811

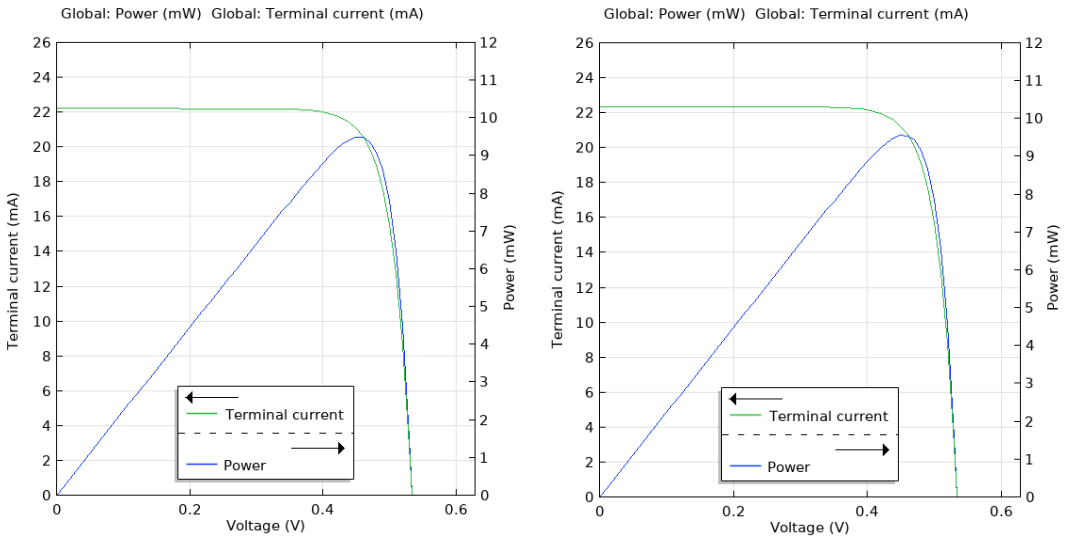

Figure 4.15 I-V and P-V curves for the 1D silicon solar cell measured at 50 ºC with the original complex refractive index (left) and adjusted complex refractive index (right)

Table 11 Solar cell's parameters for the 1D silicon solar cell for at 50 ºC with the original and adjusted complex refractive index

Refractive Index	I_{SC} $[mA]$	V_{OC} $[V]$	P_{MP} $[mW]$	FF
Original	22.23	0.533	9.50	0.802
Adjusted	22.37	0.534	9.56	0.800

As can be seen by Tables 9, 10 and 11, when the adjusted complex refractive index is taken into account, there will be some changes in the performance of the silicon solar cell. When the temperature dependent complex refractive index is inputted into the model, the behavior of the cell is closer to reality than it would be if the fixed refractive index were used, so some conclusions can be drawn about its impact on the cell. The parameter that will be most affected is the short circuit current which grows considerably more than if the complex refractive index measured at 25 ºC was considered. In the latter case, the I_{SC} increased very slightly with the temperature, with a coefficient of about +0.005 %/°C. When the temperature dependent complex refractive index is used, the coefficient is about +0.03 %/°C, which is closer to the values typically observed in real silicon solar cells. The change in the I_{SC} can perhaps be best explained due to the change in the generation rate of the charge carriers. With an increase in temperature comes an increase in the value of the extinction index which will subsequently cause an increase in the absorption coefficient, as can be seen by expression (4-3). The absorption coefficient relates how far into the semiconductor the sunlight travels before it is absorbed by the material. The higher the absorption coefficient, the shorter the length the sunlight can penetrate the semiconductor before it is abosrbed. An increase in the absorption coefficient means that the semiconductor will more readily absorb photons which will subsequently cause an increase in the generation of charge carriers, which will lead to an increase in the I_{SC}, since it is known that the I_{SC} is strongly dependent on the generation rate. On the other hand, the reflection coefficient is not uniformly or strongly affected by the temperature, meaning that the increase the real part of the complex

refractive index suffers with the temperature does not have a strong impact on the generation rate and consequently the I_{SC}. At the same time, the adjusted complex refractive index seems to have had almost no effect in the open circuit voltage of the cell (with there being only a minor discrepancy in its value for higher temperatures). The fill factor of the cell was also relatively unaffected. The slight increase in the maximum power, when the adjusted complex refractive index is taken into consideration, is expected since, for reasons stated above, there will be an increase in the current produced by the cell.

It is worthy of note that, for both the original and the adjusted complex refractive index, no wavelengths lower than 450 nm were considered in the computational simulations since, for those wavelengths, their exact dependence on the temperature could not be found in the revision of the literature. However, since it is still known that, with an increase in temperature, the real and imaginary part of the complex refractive index will grow, this in no way affects what was previously concluded about the impact the temperature will have on the complex refractive index and subsequently on the performance of the solar cell.

4.4 The Temperature Dependence of the Solar Cell's Parameters

In order to understand how the temperature affects all of the solar cell's parameters (namely the series and shunt resistance, the diode ideality factor and the reverse saturation current), an extraction of said parameters was conducted for several different temperatures and conclusions were drawn. For all 4 parameters, this extraction was made using the previously computed I-V curves. This was done for all 4 different types of cells that were previously designed in section 4.1. Computing the values for the parasitic resistances and the diode ideality factor with great accuracy from a I-V curve is a difficult process. For the determination of the parasitic resistances, the following two expressions were used, having taken care to use values as close to the points of interest (open circuit voltage and short circuit current) as possible.

$$R_S = -\frac{dV}{dI}\ (around\ V = V_{OC}) \tag{4-15}$$

$$R_{SH} = -\frac{dV}{dI}\ (around\ I = I_{SC}) \tag{4-16}$$

For the diode ideality factor, *n*, it can be approximated using two points on the slope of the I-V curve by the following expression:

$$n = \frac{V_A - V_B}{V_T \ln \frac{I_A - I_{SC}}{I_B - I_{SC}}} \tag{4-17}$$

The reverse saturation current can be approximated in the following way:

$$I_S = \frac{I_{SC}}{\left(e^{\frac{V_{OC}}{nV_T}} - 1\right)} \quad (4\text{-}18)$$

4.4.1 Silicon Solar Cell

For the silicon solar cell, in order to obtain the maximum possible accuracy in the calculations of the cell's parameters, both the adjusted band gap and complex refractive index were inputted into the model. Figures 4.16, 4.17, 4.18 and 4.19 show how the parameters vary with the temperature. The series resistance decreases with the increase in temperature, which proves beneficial to the operation of the solar cell. The shunt resistance, on the other hand, does not behave in a uniform fashion with an increase in the temperature of the cell. The values reached by the shunt resistance are, however, high enough that this does not greatly affect the performance of the silicon cell. The diode ideality factor experienced an increase up until the temperature of 45 ºC, after which it decreased. The reverse saturation current progressively increased with the temperature.

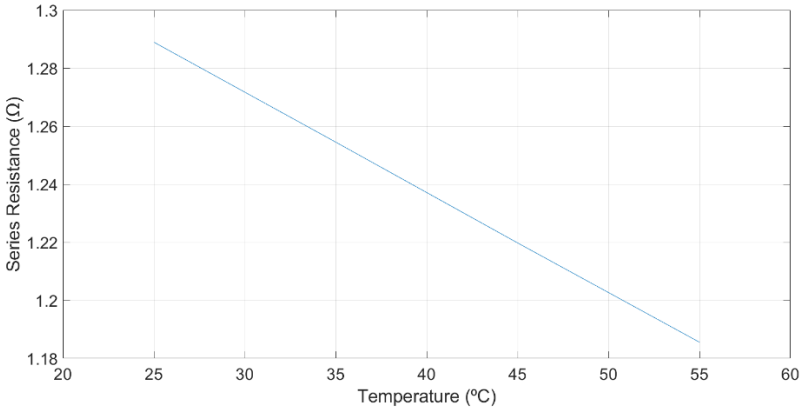

Figure 4.16 The variation of the series resistance of the 1D silicon cell with the temperature

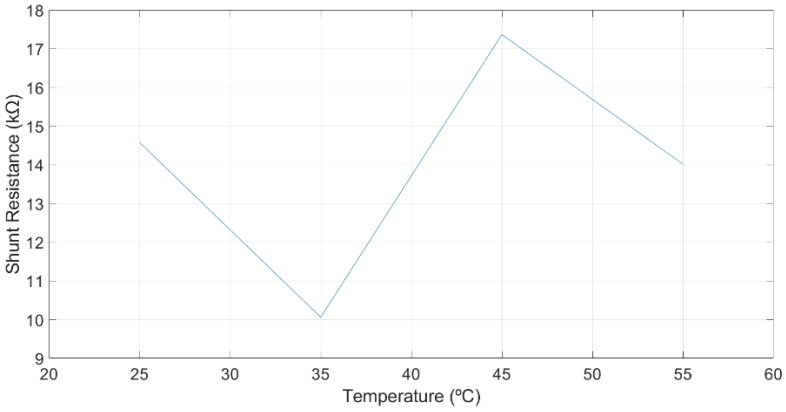

Figure 4.17 The variation of the shunt resistance of the 1D silicon cell with the temperature

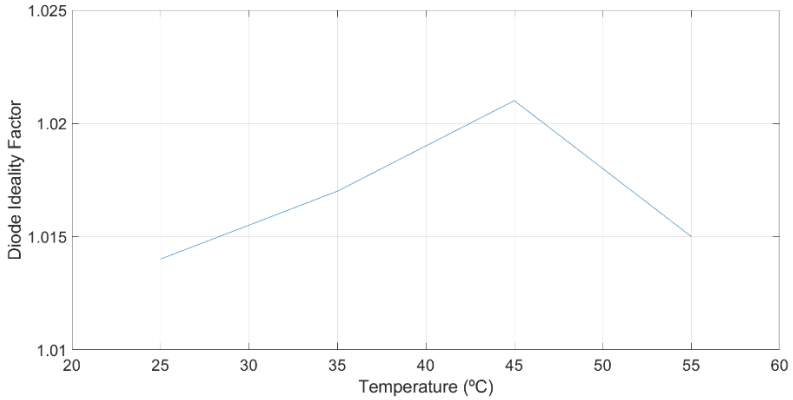

Figure 4.18 The variation of the diode ideality factor of the 1D silicon cell with the temperature

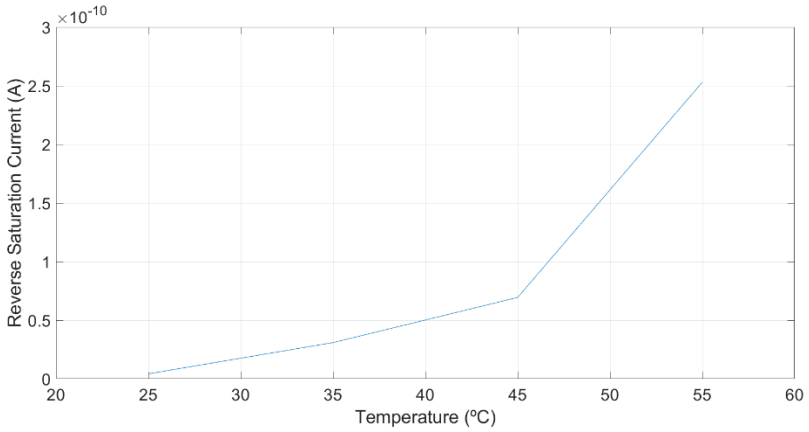

Figure 4.19 The variation of the reverse saturation current of the 1D silicon cell with the temperature

4.4.2 CIGS Solar Cell

Figures 4.20, 4.21, 4.22 and 4.23 show the effect an increase in the temperature of the semiconductor will have in the CIGS solar cell (or CIS cell to be more accurate). When it comes to the series resistance, the temperature does not seem to have a uniform effect on its value, with the value of R_S oscillating between approximately 0.7 Ω and 0.9 Ω, depending on the value of the temperature. The value of the shunt resistance on the other hand, stayed relatively consistent with the increase in temperature of the cell. The diode ideality factor experienced almost no change for temperatures below 35 ºC, noticed an increase between the temperatures of 35 ºC and 45 ºC, and afterwards decreased slightly. The reverse saturation current grew exponentially, which is to be expected for reasons previously discussed in this thesis.

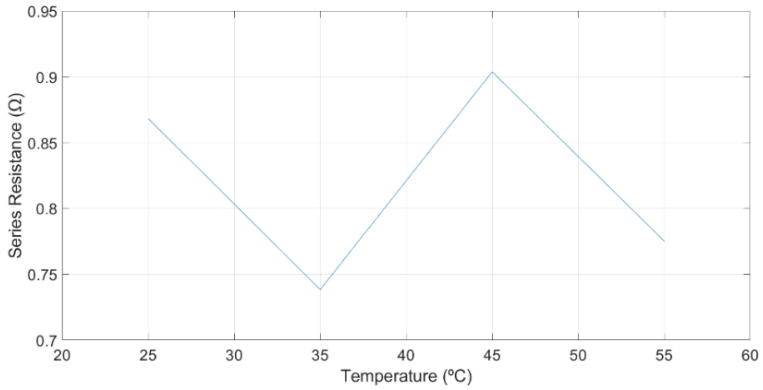

Figure 4.20 The variation of the series resistance of the 1D CIS cell with the temperature

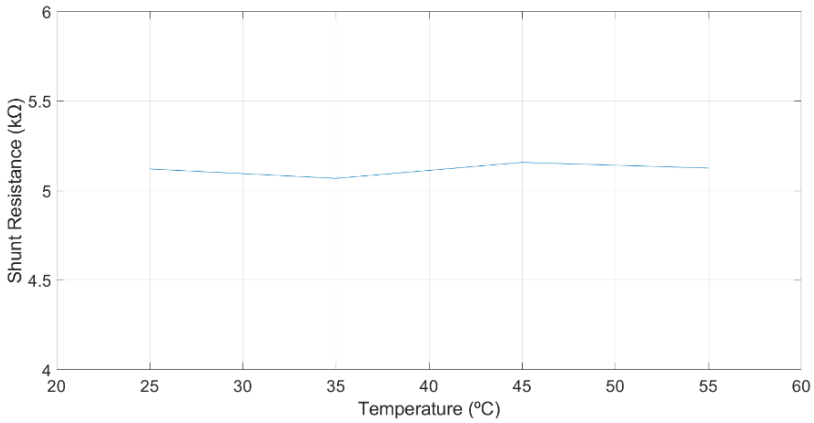

Figure 4.21 The variation of the shunt resistance of the 1D CIS cell with the temperature

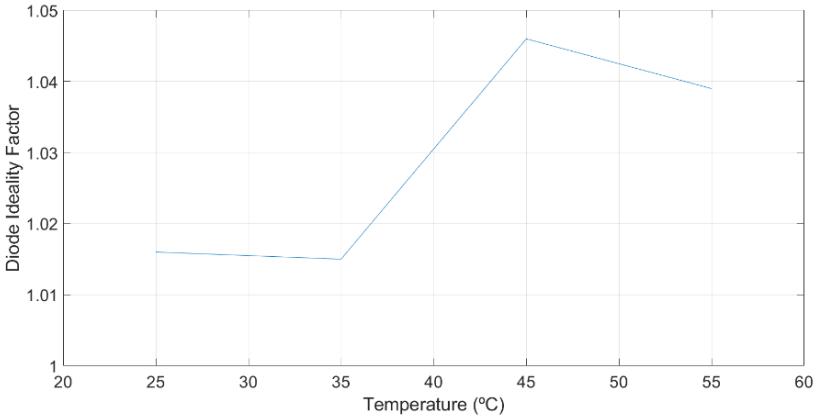

Figure 4.22 The variation of the diode ideality factor of the 1D CIS cell with the temperature

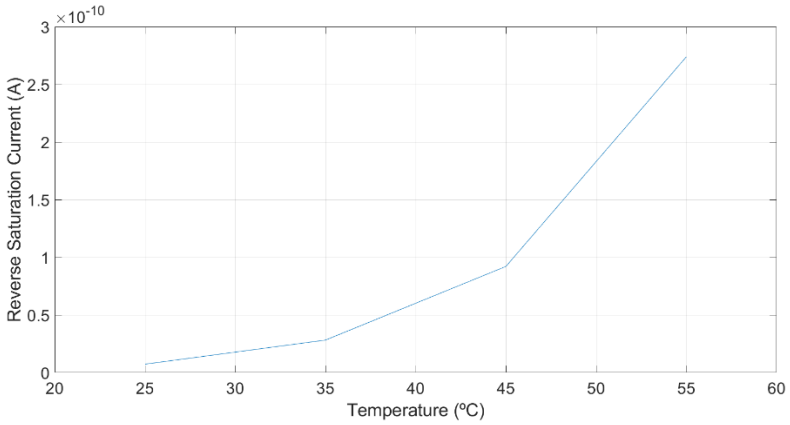

Figure 4.23 The variation of the reverse saturation current of the 1D CIS cell with the temperature

4.4.3 CdTe Solar Cell

The temperature dependence of the parameters of the Cadmium Telluride cell, can be seen in figures 4.24, 4.25, 4.26 and 4.27. An increase in the temperature lead to an increase in the series resistance, which will negatively impact the efficiency of the solar cell. When it comes to the shunt resistance, very high and similar values were registered, with there being only a slight dip when the cell was operating at 45 ºC, which can perhaps be attributed to an error in measurement. The saturation current had an expected growth with the temperature and the diode ideality factor behaved similarly than it did in the CIGS cell, having experienced a growth when the temperature of the semiconductor is between 35 ºC and 45 ºC, but being relatively uniform for the other temperatures considered.

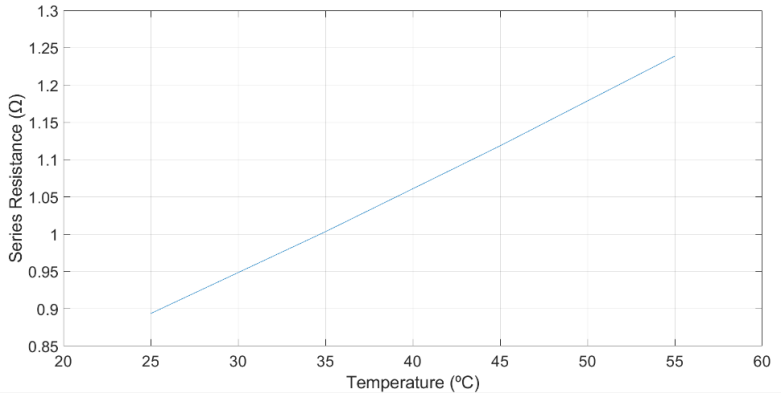

Figure 4.24 The variation of the series resistance of the 1D CdTe cell with the temperature

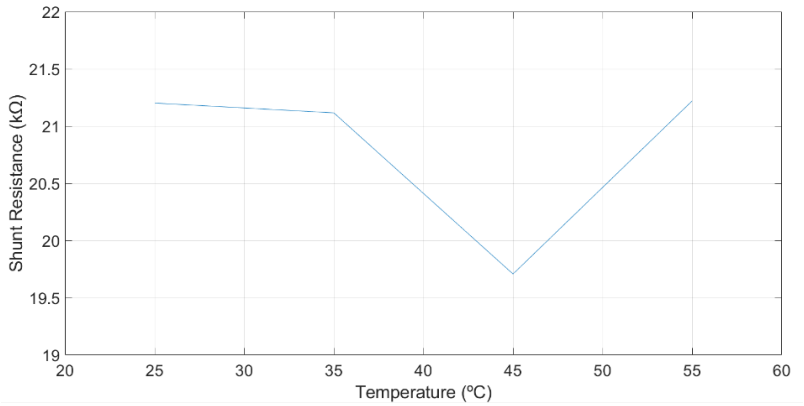

Figure 4.25 The variation of the shunt resistance of the 1D CdTe cell with the temperature

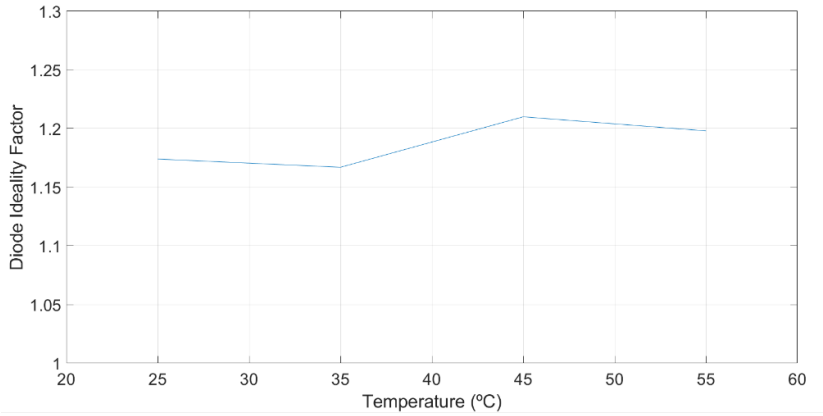

Figure 4.26 The variation of the diode ideality factor of the 1D CdTe cell with the temperature

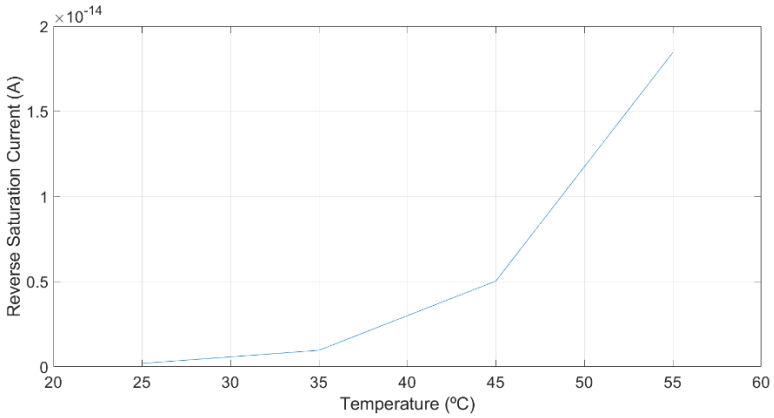

Figure 4.27 The variation of the reverse saturation current of the 1D CdTe cell with the temperature

4.4.4 Perovskite Solar Cell

Finally, the perovskite solar cell's parameters were computed and their dependence on the temperature was traced, as can be seen in the figures 4.28, 4.29, 4.30 and 4.31. Just like in the CIGS cell, the series resistance oscillated with the temperature, making it hard to draw conclusions about the impact the temperature had on this parameter. With an increase in the temperature of the cell the shunt resistance progressively increased, which is beneficial to the operation to the solar cell. The diode ideality factor behaved similarly with the other cells,

achieving low values and having an uneven behavior with the increase in temperature. The reverse saturation current had an expected increase with the temperature.

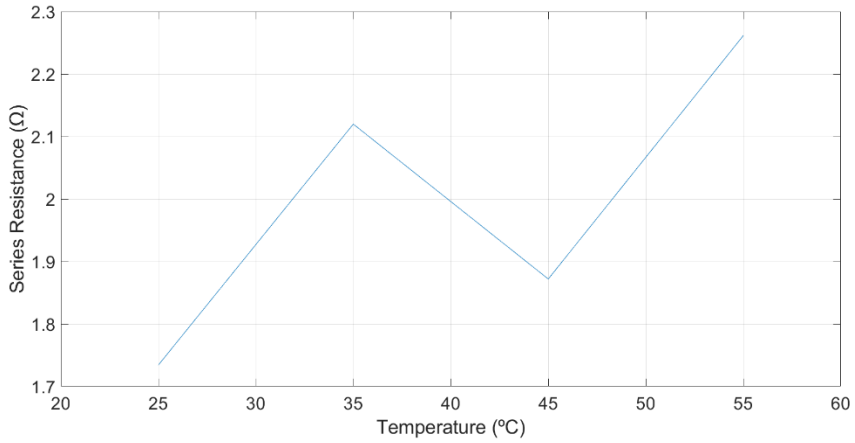

Figure 4.28 The variation of the series resistance of the 1D Perovskite cell with the temperature

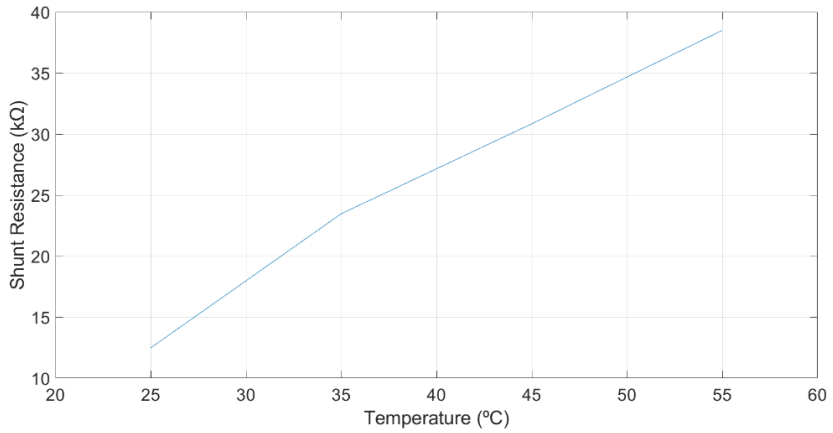

Figure 4.29 The variation of the shunt resistance of the 1D Perovskite cell with the temperature

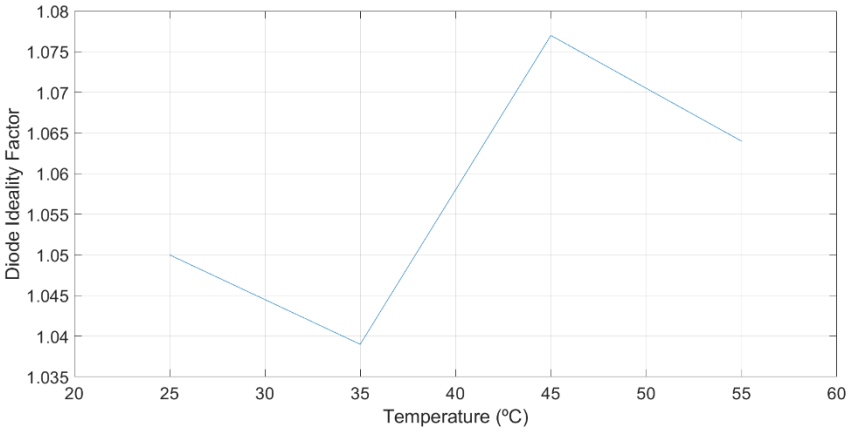

Figure 4.30 The variation of the diode ideality factor of the 1D Perovskite cell with the temperature

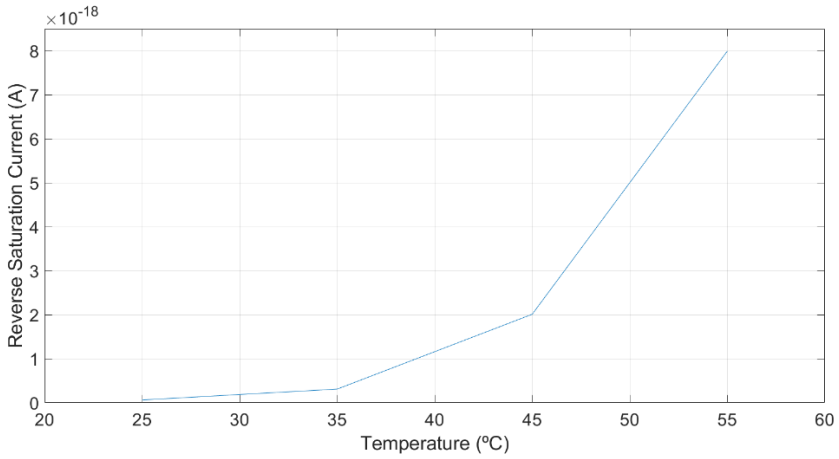

Figure 4.31 The variation of the reverse saturation current of the 1D Perovskite cell with the temperature

A further study of the impact the temperature will have on these parameters is recommended, since there may be some differences between the results obtained here, and what the results would be for commercial cells. When it comes to the parasitic resistances, it is possible that their behavior with the temperature will vary in commercial cells, but, in any case, the change that they will experience with the temperature will most likely be negligible in the overall performance of the solar cell. The diode ideality factor is expected to reach higher values in commercial cells. The low values reached by the ideality factor in the computational simulations indicate that the recombination processes are occurring in the bulk areas of the devices (meaning not in p/n junction), which may not necessarily be the case in commercial cells. For all 4 solar cells, the reverse saturation current increased exponentially with the temperature which is in accordance with the literature on the subject, and which explains the decrease in the open circuit voltage.

4.5 2D Silicon Solar Cell

A two-dimensional model of a silicon solar cell was designed and implemented on the a finite element simulation software. By using a 2D model, a more accurate representation of the behavior of the silicon a solar cell can be studied since, now, the width of the cell is considered in the computations. Just like in the one-dimensional models, relevant data about silicon, such as the band gap, the refractive index and the effective density of states was introduced to the model. In order to perform the simulations, it was now necessary to not only use the semiconductor module, but also a heat transfer in solids module, which made it necessary to introduce into the program data about silicon such as the thermal conductivity, the density and the heat capacity at constant pressure. The doping and metal contacts were done in much the same way as in the 1D model, by using the top and bottom layers of the 2D cell. For the solar spectrum, once again, an approximation of the AM1.5 Global spectrum was used. The geometry of the 2D cell can be seen in Figure 4.32.

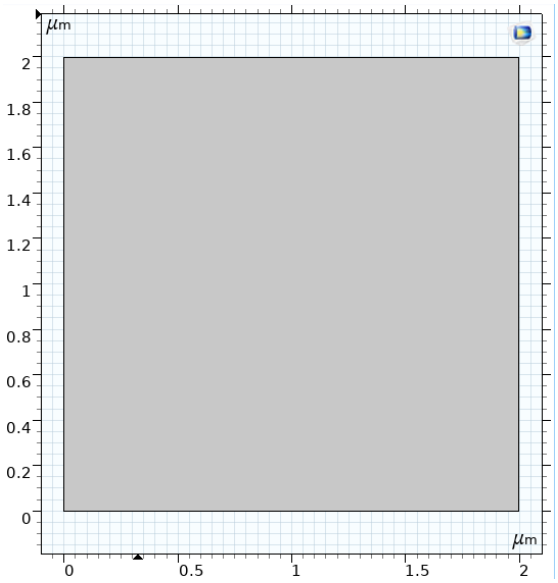

Figure 4.32 Geometry of the 2D Silicon Solar Cell

In order to compare the behavior of the 2D cell with the temperature, with the previously used 1D cell, several tests were conducted. First, the 2D cell was tested at 4 different temperatures and the corresponding I-V and P-V curves were traced, allowing for some conclusions to be drawn. In all 4 cases, the temperature was uniform all over the cell. Figures 4.33, 4.34 and Table 12 show the results of the computations.

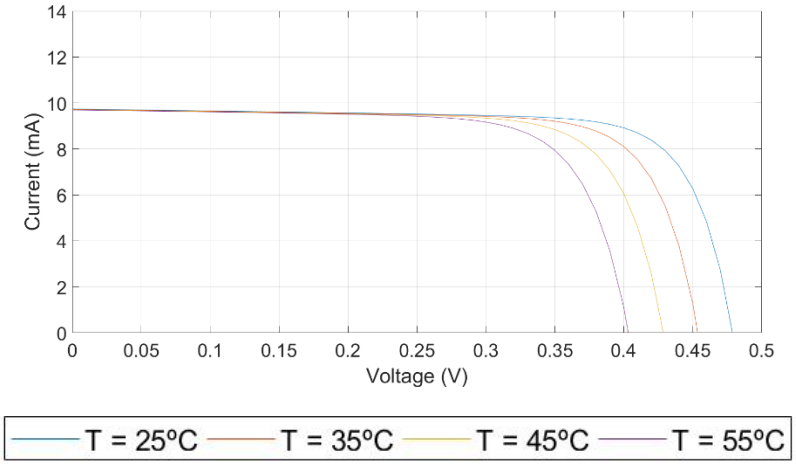

Figure 4.33 I-V curves for the 2D silicon solar cell for 4 different temperatures

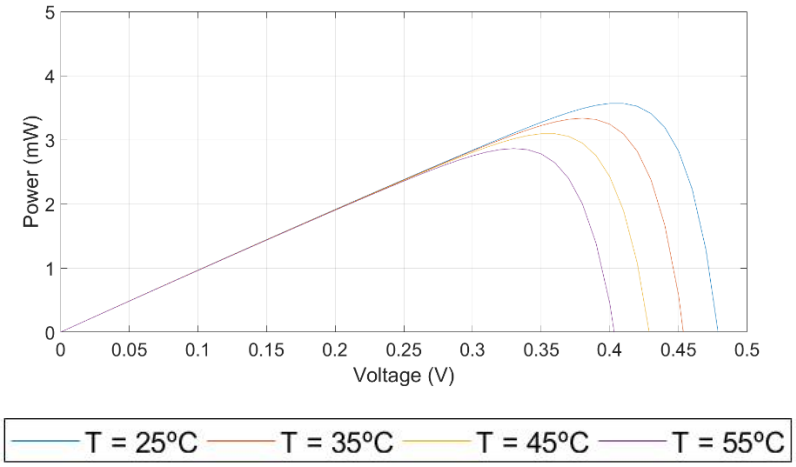

Figure 4.34 P-V curves for the 2D silicon solar cell for 4 different temperatures

Table 12 Solar cell parameters' data for the 2D silicon solar cell for 4 different temperatures

T[ºC]	I_{SC} [mA]	V_{OC} [V]	P_{MP} [mW]	FF
25	9.74	0.480	3.58	0.766
35	9.72	0.455	3.34	0.755
45	9.71	0.430	3.11	0.745
55	9.69	0.404	2.87	0.733

As can be seen in Table 12, with an increase in temperature, several changes occurred in the behavior of the silicon solar cell. The open circuit voltage and maximum power decreased with the temperature, which is expected, although the decrease was more pronounced than it was in the 1D model. The V_{OC} had a temperature coefficient of around -0.52 %/ºC and the P_{MP} had a temperature coefficient of about -0.67 %/ºC. The short circuit current experienced a slight decrease, which is contrary to what was observed on the 1D model, and in most commercial silicon solar cells. The temperature coefficient was approximately -0.02 %/ºC. The decrease in the value of the I_{SC} can perhaps be best explained by the higher degrees of recombination that occur in the 2D model. The temperature coefficient of the fill factor, on the other hand, was not much different than in the 1D model, being around -0.14 %/ºC.

4.5.1 The Temperature Dependence of the Band Gap

Just like in the 1D model, a study of the impact the temperature dependent band gap will have on the cell's performance was conducted. Just as before, I-V and P-V curves were computed using the fixed band gap value of 1.121 eV and the more accurate calculated band gap. Figures 4.35, 4.36 and 4.37 show the results of the computations.

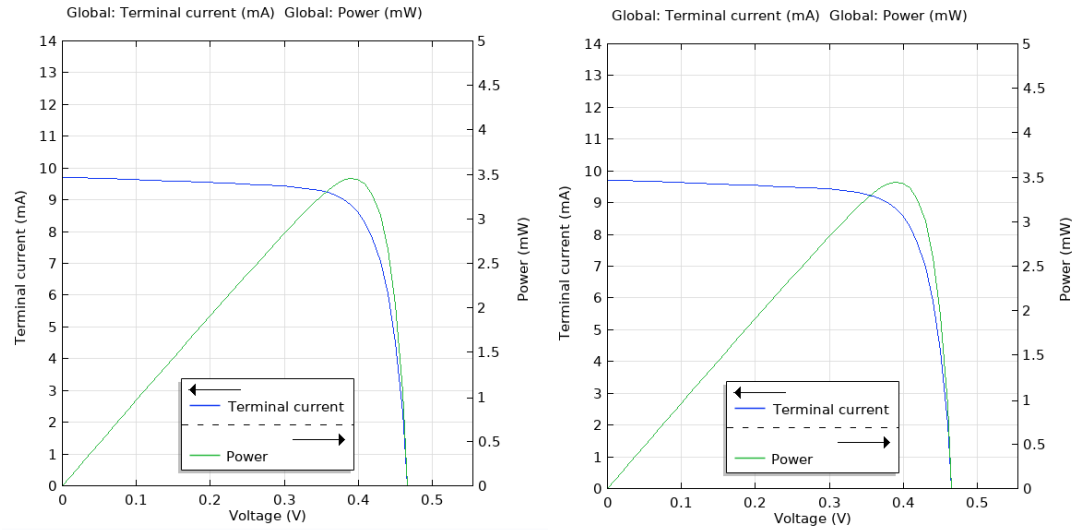

Figure 4.35 I-V and P-V curves for the 2D silicon solar cell measured at 30 ºC with a band gap of 1.121 eV (left) and 1.120 eV (right)

Table 13 Solar cell's parameters for the 2D silicon solar cell for 2 different band gaps measured at 30 ºC

$E_g(30)[eV]$	$I_{SC}\ [mA]$	$V_{OC}\ [V]$	$P_{MP}\ [mW]$	FF
1.121	9.73	0.467	3.46	0.761
1.120	9.73	0.466	3.45	0.761

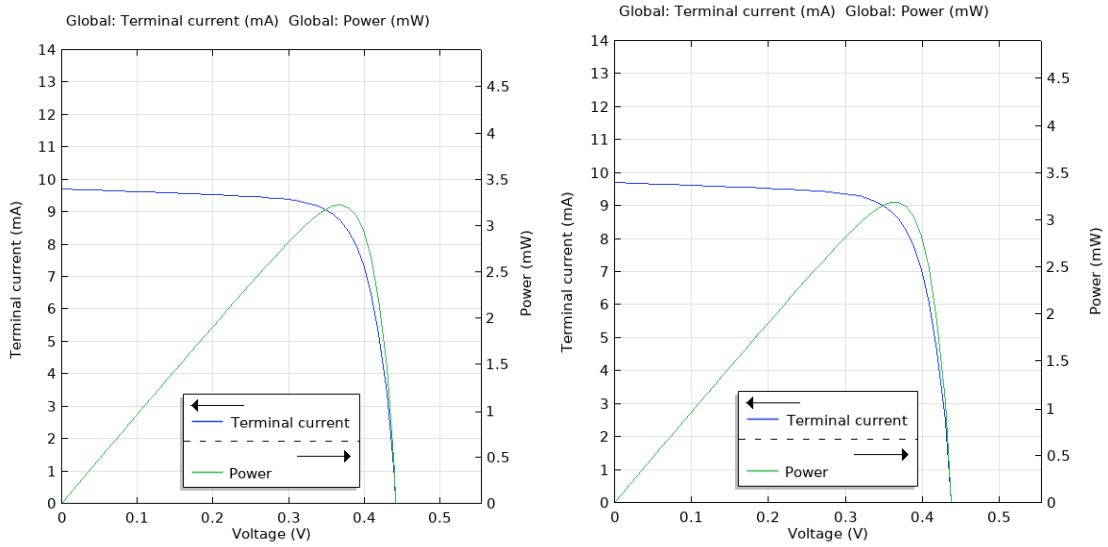

Figure 4.36 I-V and P-V curves for the 2D silicon solar cell measured at 40 ºC with a band gap of 1.121 eV (left) and 1.117 eV (right)

Table 14 Solar cell's parameters for the 2D silicon solar cell for 2 different band gaps measured at 40 ºC

$E_g(40)[eV]$	$I_{SC}\ [mA]$	$V_{OC}\ [V]$	$P_{MP}\ [mW]$	FF
1.121	9.72	0.442	3.23	0.752
1.117	9.71	0.438	3.19	0.750

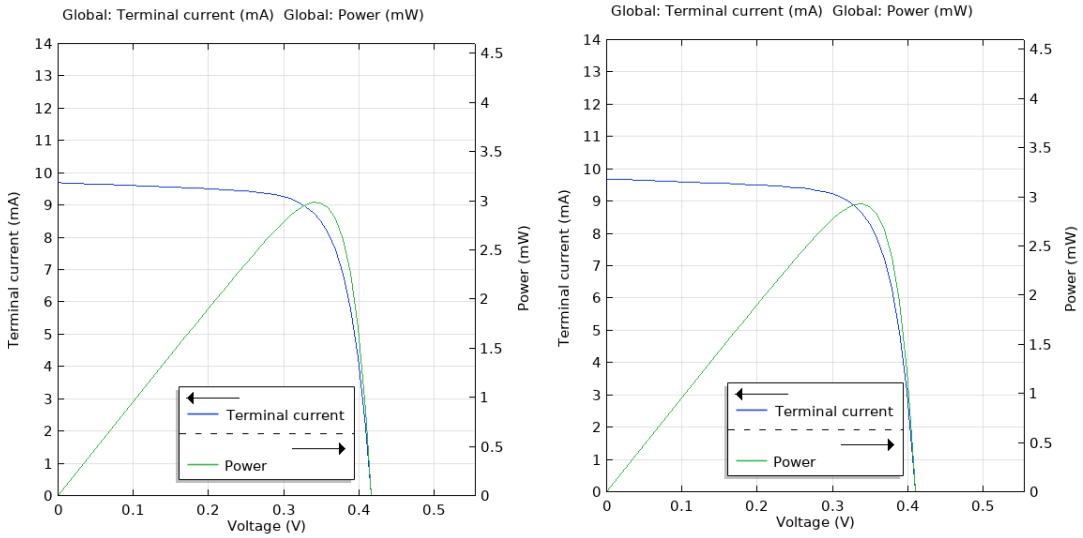

Figure 4.37 I-V and P-V curves for the 2D silicon solar cell measured at 50 ºC with a band gap of 1.121 eV (left) and 1.115 eV (right)

Table 15 Solar cell's parameters for the 2D silicon solar cell for 2 different band gaps measured at 50 ºC

$E_g(50)[eV]$	$I_{SC}\ [mA]$	$V_{OC}\ [V]$	$P_{MP}\ [mW]$	FF
1.121	9.70	0.417	2.99	0.739
1.115	9.70	0.411	2.94	0.737

In the two-dimensional cell, the temperature dependent band gap impacted the solar cell in much of the same way that it did in the 1D model. When the more accurate band gap is inputted into the model, there will be a decrease in the open circuit voltage and maximum power of the cell, which is caused by the, previously discussed, changes in the intrinsic carrier concentration. The short circuit current and the fill factor were, once again, little affected by the change in band gap. The more accurate temperature coefficient of the V_{OC} was - 0.58 %/ºC and for the P_{MP} it was approximately -0.72 %/ºC. The change in the temperature coefficients was slightly more pronounced for the V_{OC} but virtually the same for the P_{MP}.

4.5.2 The Temperature Dependence of the Refractive Index

Next, the temperature dependent complex refractive index was inputted into the model, and the I-V and P-V curves were computed. The resulting curves were then compared to what they would be like if the complex refractive index taken at 25 ºC was considered instead. Figures 4.38, 4.39 and 4.40 and Tables 16, 17 and 18 show the results.

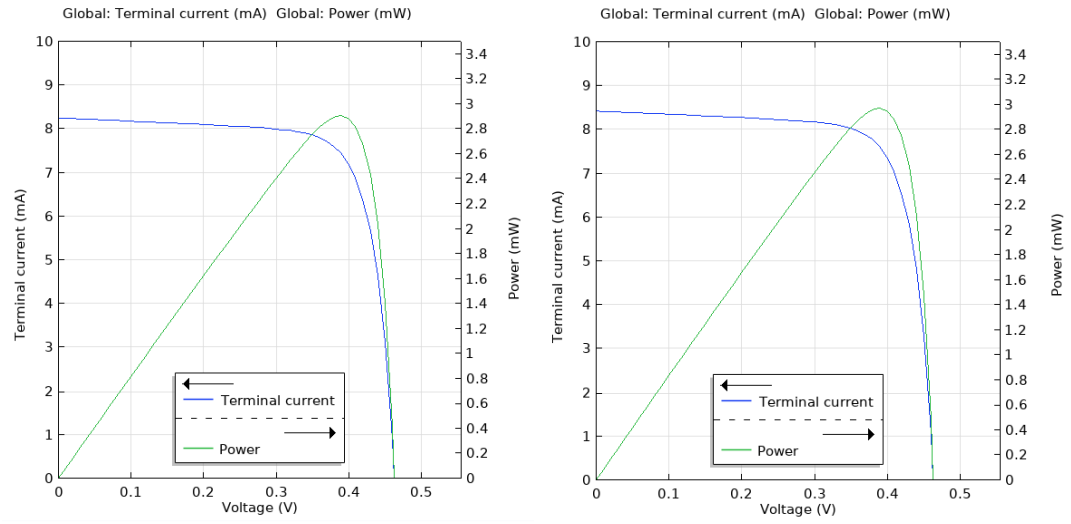

Figure 4.38 I-V and P-V curves for the 2D silicon solar cell measured at 30 ºC with the original complex refractive index (left) and adjusted complex refractive index (right)

Table 16 Solar cell's parameters for the 2D silicon solar cell for at 30 ºC with the original and adjusted complex refractive index

Refractive Index	$I_{SC}\ [mA]$	$V_{OC}\ [V]$	$P_{MP}\ [mW]$	FF
Original	8.25	0.463	2.91	0.762
Adjusted	8.43	0.463	2.97	0.761

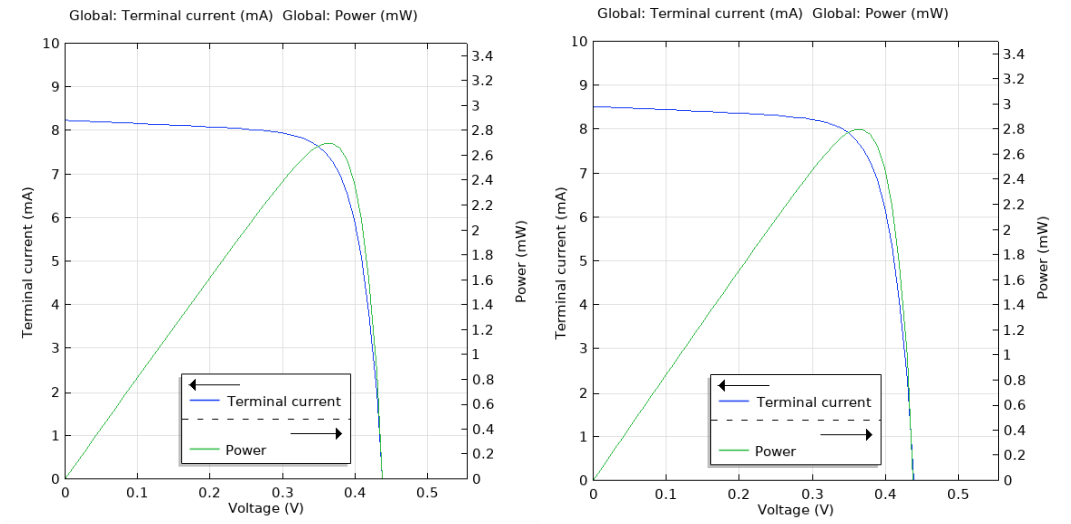

Figure 4.39 I-V and P-V curves for the 2D silicon solar cell measured at 40 ºC with the original complex refractive index (left) and adjusted complex refractive index (right)

Table 17 Solar cell's parameters for the 2D silicon solar cell for at 40 ºC with the original and adjusted complex refractive index

Refractive Index	$I_{SC}\ [mA]$	$V_{OC}\ [V]$	$P_{MP}\ [mW]$	FF
Original	8.24	0.438	2.70	0.748
Adjusted	8.53	0.439	2.80	0.748

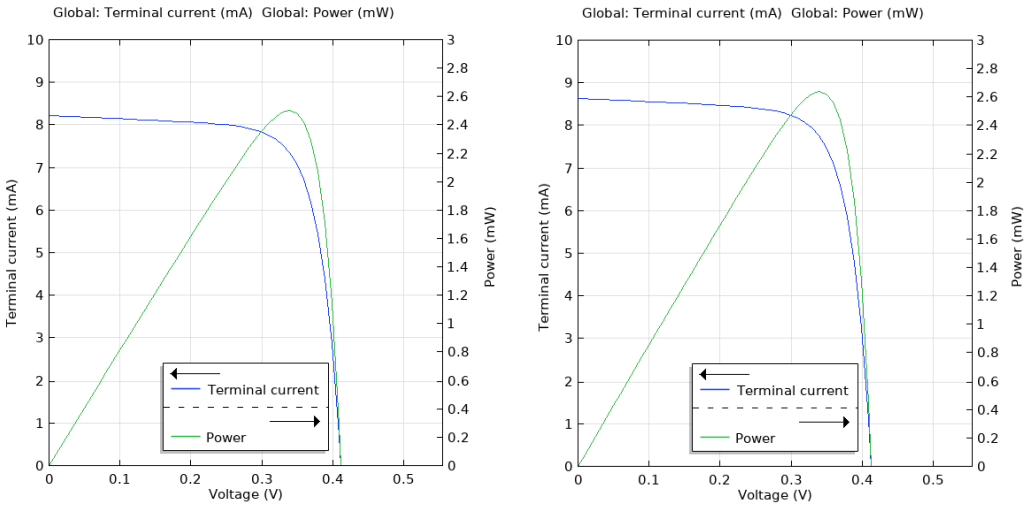

Figure 4.40 I-V and P-V curves for the 2D silicon solar cell measured at 50 ºC with the original complex refractive index (left) and adjusted complex refractive index (right)

Table 18 Solar cell's parameters for the 2D silicon solar cell for at 50 ºC with the original and adjusted complex refractive index

Refractive Index	I_{SC} $[mA]$	V_{OC} $[V]$	P_{MP} $[mW]$	FF
Original	8.23	0.412	2.50	0.737
Adjusted	8.64	0.414	2.64	0.738

When the adjusted complex refractive index is taken into consideration, the short circuit current, now, experiences a growth with the temperature, which aligns with the usual behavior of silicon solar cells. The reasons for this, as was explained before, have to do with the absorption coefficient and the generation of charge carriers. The temperature coefficient of the I_{SC} is now positive, instead of negative, being approximately +0.11 %/ºC which is higher than the traditionally I_{SC} coefficient for silicon cells. The reason why the values of the I_{SC} are overall lower than they were when the 2D solar cell was first simulated, is because not all wavelengths of the incident sunlight are being considered. This does not, however, affect any of the general conclusions that were drawn about the behavior of the I_{SC} with the extinction index. Unlike the 1D model, the open circuit voltage is slightly higher if the adjusted complex refractive index is used, rather than the original, showing that the more accurate temperature coefficient of the V_{OC} is not quite as pronounced as was previously reported. The increase in the maximum power is easily explained by the growth in the short circuit current and open circuit voltage.

4.5.3 The Temperature Dependence of the Solar Cell's Parameters

Finally, the parasitic resistances, the diode ideality factor and the reverse saturation current, measured for 4 different temperatures, were computed for the 2D silicon solar cell. Figures 4.41, 4.42, 4.43 and 4.44 show the results of the computations. Comparing the values of the parameters and their temperature dependence with the 1D cell model, some discrepancies become apparent. When it comes to the series resistance, in the 2D model, with an increase in temperature there will be an increase in the value of R_S, which is the opposite of what happened in the 1D model. The overall value of the R_S is also slightly larger. The shunt resistance experienced a slight decrease with the temperature, rather than the oscillatory nature that it had shown in the 1D model. The overall values were also much lower in the 2D model, which means that the R_{SH} will have a more negative impact on the performance of the silicon cell. The diode ideality factor decreased with the temperature and achieved higher values than it did in the 1D model, which is in accordance with most of the literature regarding silicon cells. The higher values of the ideality factor indicate that, in the 2D model, more recombination is occurring inside the p/n junction. The reverse saturation current had an expected growth with the temperature, achieving higher values than it did in the 1D model.

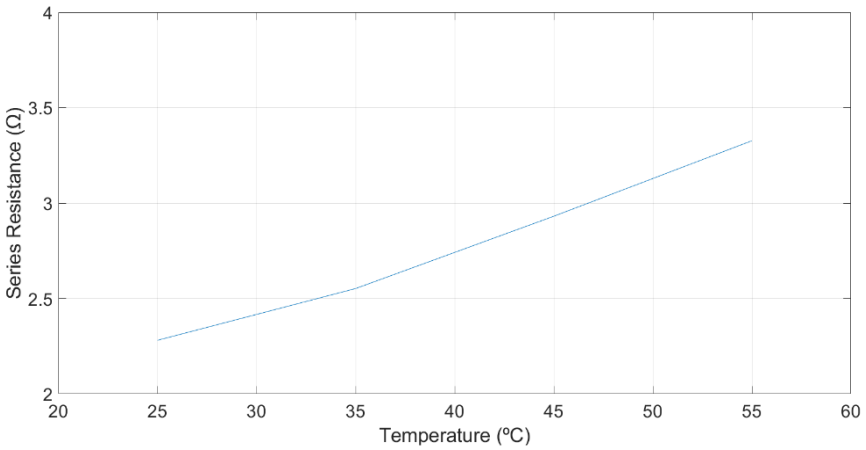

Figure 4.41 The variation of the series resistance of the 2D silicon cell with the temperature

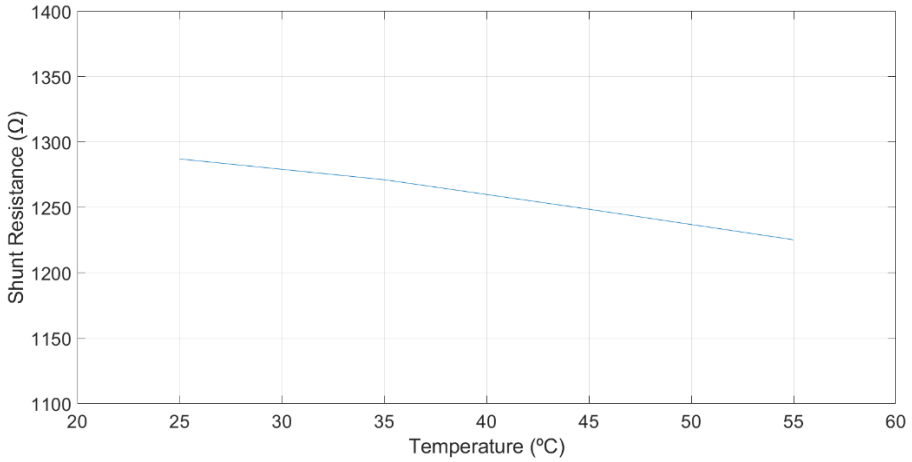

Figure 4.42 The variation of the shunt resistance of the 2D silicon cell with the temperature

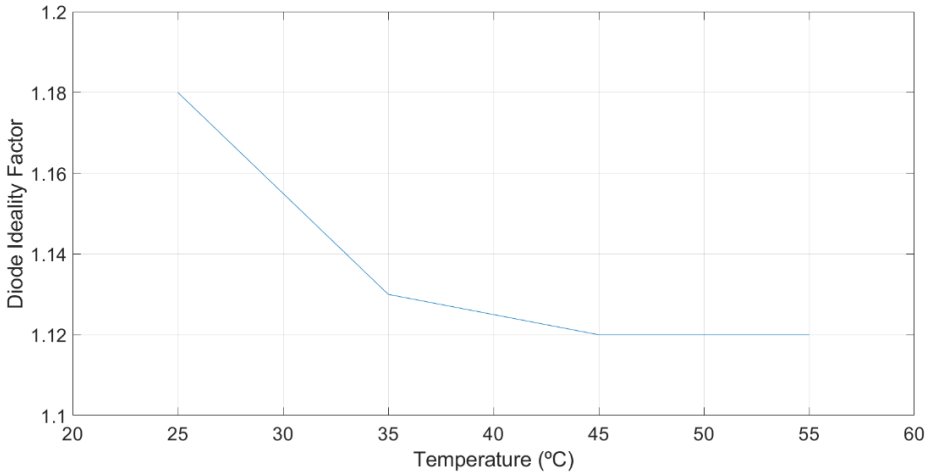

Figure 4.43 The variation of the diode ideality factor of the 2D silicon cell with the temperature

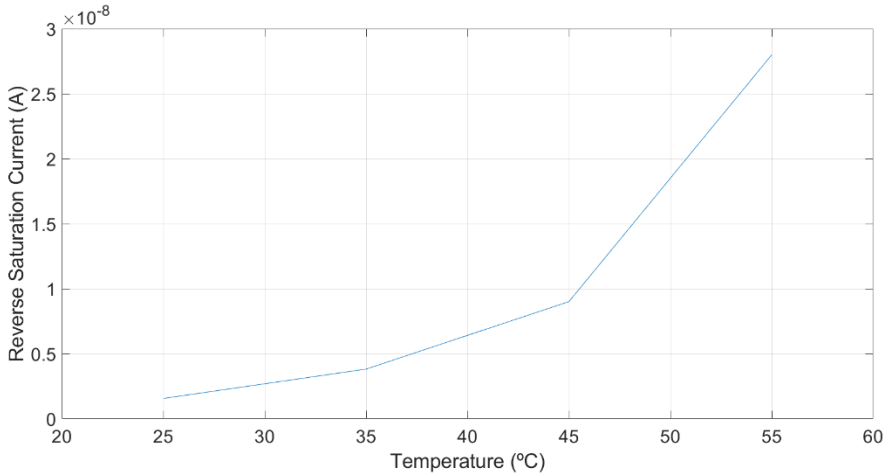

Figure 4.44 The variation of the reverse saturation current of the 2D silicon cell with the temperature

5. Cooling Methods

Having already established the negative impact that the temperature will have on the performance of photovoltaic systems, some solutions are now proposed, intended for the reduction of this negative effect. A review of the literature was conducted, where several ways of using the unnecessary heat generated in the panel, or of cooling the photovoltaic system were analyzed and studied.

5.1 Photovoltaic Thermal Collector

Photovoltaic/thermal (PV/T) collectors, also known as hybrid solar collectors, are units comprised of a photovoltaic system, which will convert sunlight into electricity, and a solar thermal collector which will convert sunlight into thermal energy. By using a PV/T collector it is possible not only to cool the photovoltaic system, but also to extract the unnecessary heat produced by the PV system, which will then be converted into useful energy. Because of this, the conversion efficiency reached by PV/T collectors are much higher than those reached by PV systems (being as high as 80%), while also having the additional benefit of extending the lifetime of the solar cells in the PV system, since they will not suffer as much heat degradation. A typical PV/T collector consists of a PV module which is installed on top of a heat absorber on top of an insulator. The waste heat produced by the PV system will be transferred to a heat transfer fluid. The heat transfer fluid can be a gas or a liquid which is responsible for cooling the PV module and transporting and storing the thermal energy. Depending on the heat transfer fluid used, the PV/T collectors can be broadly divided into two following categories: PV/T air collector and PV/T liquid collector.

In PV/T air collectors, the air channel may be above or below the PV system, in a single or double pass. Figure 5.1 shows a cross-section of two types of PV/T air collectors, one a single pass PV/T air collector where the air channel is located below the PV system, the other a double-pass PV/T air collector.

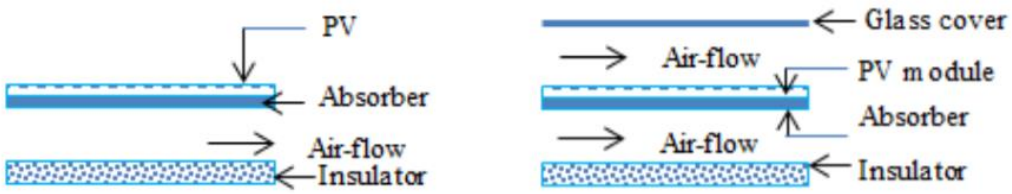

Figure 5.1 Cross-section of a single pass PV/T air collector (left) and a double pass PV/T air collector (right) [29]

PV/T air collectors have several advantages, the main one being that they are relatively cheap and easy to manufacture. They also do not require any thermal collecting materials attached to the PV system. On the other hand, since the air has a low heat capacity and low heat conductivity, the heat transfer will not be very pronounced and consequently the PV/T air collectors will not have a very high efficiency. There are several ways of improving the efficiency

of a PV/T air collector. One such method [30] includes attaching metal fins to the rear of the PV module, and perpendicular to the air flow, which will cause a greater cooling of the photovoltaic system and a greater heat transfer rate, thereby increasing the efficiency of the collector, although with them also come additional concerns when it comes to the cost and complexity of the system.

PV/T liquid collectors are more efficient than PV/T air collectors, but have several disadvantages, one of them being their higher manufacturing cost and maintenance. In a typical PV/T liquid collector, a working fluid (such as water) circulates in the heat absorber, behind the PV module. The working fluid will absorb the heat and therefore the temperature of the photovoltaic system will lower. As was previously mentioned, the efficiency of PV/T liquid collectors is higher than PV/T air collectors, since the liquid used (typically water) has a higher heat conductivity and heat capacity, resulting in a higher volume of heat transfer and consequently an increase in the efficiency of the system. Unlike PV/T air collectors, however, in PV/T liquid collectors it is possible for the liquid to boil or freeze which will impact the efficiency of the system. It is also possible for there to be leakage of the fluid which will cause damage to the collector. The cross-view of a typical PV/T water collector can be seen in figure 5.2.

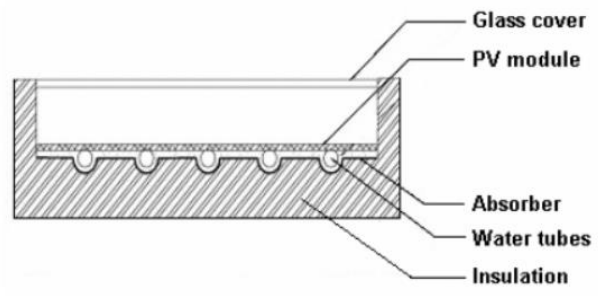

Figure 5.2 Cross-section of a PV/T water collector [31]

5.2 Phase Change Material

A method that may be used to cool the photovoltaic system, and thereby increase its efficiency, is the installation of phase change materials (PCMs) on the back of the solar panels. Phase change materials are substances that undergo a reversible transition of phase (usually between the solid and liquid states), while absorbing or rejecting heat in the process. PCMS are, usually, either organic materials derived from petroleum or salt hydrates. Figure 5.3 shows a typical PV module with a PCM layer attached to the backside of the panel.

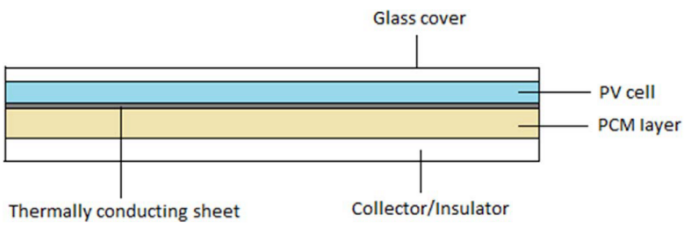

Figure 5.3 Cross-section of a PV module with a PCM layer attached at the rear [32]

Phase change materials have the advantage of having several times more heat capacity than water or air based systems and are able to store heat which can subsequently be used for other purposes [32]. They also have the added advantage of being able to delay the temperature rise in the photovoltaic system without any electricity consumption or requiring maintenance. Some of their disadvantages include a large initial investment, corrosiveness, and the fact that they tend to perform better in hot climatic conditions [33]. The absorbing qualities of the PCMs will also degrade over time.

When it comes to the selection of the phase change material, one parameter that must be considered is the melting point of the PCM. PCMs with lower melting temperatures will be able to maintain the desired temperature of the photovoltaic system for only short amounts of times and will become ineffective during the hottest parts of the day. For PCMs with higher melting temperatures, they will not be able to maintain the solar panel at temperatures as cool as PCM with lower melting temperatures, but they will be able to maintain the PV system beneath a certain temperature for a longer period of time, preventing the creation of hot stops [32]. The choice of the PCM will depend on the peak temperature that can be reached by the photovoltaic system and the type of solar panel that was used.

5.3 Water Immersion

A method that may be employed in order to cool the photovoltaic system is the immersion of the solar panel in a body of water. This technique has some advantages as well as some drawbacks. Aside from the natural effects that the cooling will have on the efficiency of the PV system, immersing the panel in water will also cause a reduction in the light reflection which will prove beneficial for the efficiency [34]. The efficiency of the solar panel will also depend on the depth into which it is immersed in the water. Figure 5.4 shows the variation of the efficiency of a polycrystalline silicon solar panel in relation to the depth into which it is immerged in a body of distilled water.

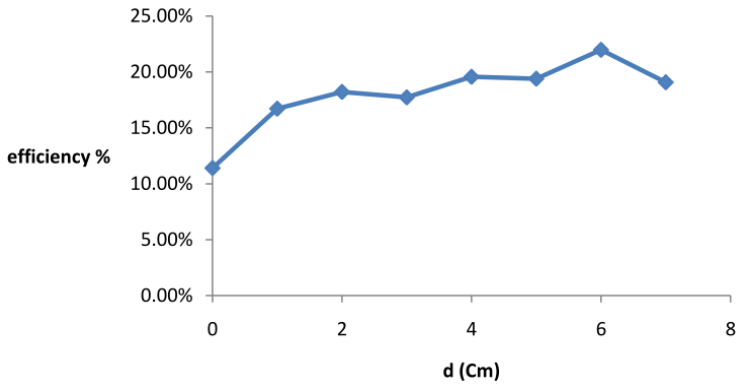

Figure 5.4 Efficiency of a polycrystalline silicon solar panel as a function of the depth of the water immersion [34]

Immersing the solar panel in water is an efficient and environment-friendly process, although consideration also has to be taken, since the complexity and cost of this cooling technique can be quite high. The efficiency of the submerged solar panel will also not be as high during cloudy days and the prolonged exposure of the panel to ionized water will eventually decrease its maximum efficiency [33].

5.4 Water Spraying

A similar method to the water immersion, is the cooling of the solar panel by the continuous flow of water over the front surface of the panel. This technique will not only reduce the temperature of the panel, but also, due to the refractive index of the water, the refection losses of the panel [35]. Unlike the water immersion method, in order to implement this method, a pump is necessary, in order to transport the water from a tank that is located below the photovoltaic module into another that is located on top of the PV system. From there, the water will flow from a series of nozzles over the front surface of the panel creating a continuous thin film of water over the panel [35]. This continuing water flow has the added advantage of, while keeping the solar panel cool, also making it clean from dust and other particles that negatively affect the performance of the panel. Figure 5.5 shows the water flowing from a series of nozzles and covering the front surface of the solar panel.

Figure 5.5 Creation of the thin film of water over the PV module by a series of nozzles [35]

Also, like the water immersion method, water spraying of the solar panel is not the most overall efficient technique since the excess heat generated by the panel, and cooled by the water, will not be used for other applications. This cooling method will also require a higher degree of maintenance and a higher cost due to the pumping power that will be necessary to ensure the cooling of the panel.

5.5 Transparent Coating

The front surface of the PV module may be covered by a visibly transparent photonic crystal thermal blackbody, where the main constituent of the photonic material will be silica (SiO_2). When this blackbody is placed on top of the solar panel, it will reflect heat generated by the panel, while, at the same time, not negatively affecting the sunlight absorption [36]. The cooling that the panel will experience may lower its temperature as much as 13 ºC, according to one study [36]. Unlike photovoltaic thermal collectors or phase change materials however, this cooling method does not take advantage of the heat generated, although the use of a transparent blackbody over the panel has the advantage of being economically feasible and not requiring any additional space.

5.6 Thermoelectric Cooling

In order to cool the photovoltaic system, it is possible to attach a thermoelectric cooling (TEC) module to the rear of the panel. A TEC module is an energy converter made up of two different semiconducting thermoelements which are wired electrically in series and thermally in parallel. When a voltage is applied to the thermoelectric module, an electric current will flow through the device which will cause a transfer of heat from one side of the TEC module to the other side, so that one side of the TEC module will be cooler while the other side will be hotter. The “hotter” side will be connected to a heat sink which will dissipate the thermal energy into the environment. A diagram showcasing the operation of a standard thermoelectric module is shown in Figure 5.6.

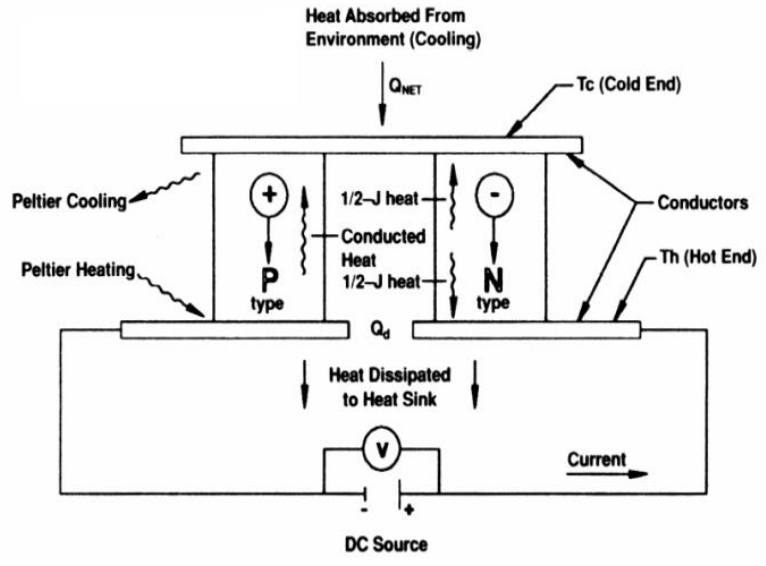

Figure 5.6 Working of Thermoelectric Module [37]

Using a thermoelectric cooler to decrease the temperature of a photovoltaic system has some drawbacks, the main ones being the fact that TEC modules will consume more power than most cooling systems, while at the same time, having a low conversion efficiency rate [38]. On the other hand, TEC modules have the advantage of being more economical than other cooling systems. They also have the added benefit of being noiseless in operation, having no moving mechanical parts, having a long working life, and requiring little maintenance [38].

6. Conclusion

6.1 Conclusions and Future Work

In this thesis, an analysis of the impact the temperature will have on the performance of solar cells was conducted. This study was important to conduct given the fact that temperature is one of the most important factors that affect the behavior of solar cells and, with its increase, overheat will be generated and the efficiency of the cell will drop. In order to better understand this effect, a theoretical study of the processes behind the operation of a solar cell was carried and various computational simulations were performed.

In terms of the theoretical analysis that was done, it was found that the temperature will mainly affect the performance of solar cells due to the impact the temperature will have on the effective density of states and the band gap of the semiconductor, which will subsequently increase the intrinsic carrier concentration. This increase will be responsible for a decrease in the open circuit voltage which is the parameter most affected by the temperature and which will be primarily responsible for the decrease in the maximum power and efficiency of the cell.

Using a finite element simulation software, and resorting to 1D models, comparisons between the performance of different solar cells in function of the temperature were made. It was found that perovskite solar cells are the least negatively affected by an increase in temperature, performing better than CdTe and CIGS cells. Silicon solar cells are, of all the cells tested, the ones who perform worse with an increase in temperature.

For the 1D silicon solar cell model, it was found that the decrease the band gap suffers with the temperature, mainly affects the open circuit voltage, while the increase the extinction index undergoes with the temperature will cause an increase in the short circuit current which slightly contributes to a better performance by the cell.

By using a 2D model of the silicon solar cell it was intended to more accurately represent the behavior of a real cell. The simulations done with this model show similar effects of the temperature on the I-V and P-V curves, with the only differences being slightly more pronounced decreases in the open circuit voltage and maximum power and a slight decrease of the short circuit current with the temperature instead of a slight increase. When it comes to the effect of the band gap and the complex refractive index, their impact was much the same as it was in the 1D model.

The review of the cooling systems that may be employed in order to lower the temperature of the photovoltaic system show that the choice of the cooling system will depend on whether the customer wishes to make use of the excess heat, the budget of the customer and the location of the installation of the PV module.

The principal advantage of doing computational simulations to study the behavior of solar cells was that it was possible to completely isolate the impact the temperature will have, by

keeping other external factors, such as the irradiance, constant. Since this will not be the case in commercial cells, further studies into the performance of cells under real conditions are recommended in order to better understand how they will be affected by the temperature. Also recommended, are further studies into the band gap, complex refractive indexes, and effective density of states of semiconductors other than silicon, since there seems to be a scarcity of published literature on the subject. Furthermore, since the impact the temperature will have on parameters of the solar cell such as the parasitic resistances and the ideality factor are not well studied, especially for non-silicon cells, more research into this area is recommended, both from a theoretical and experimental viewpoint.

Bibliography

[1] “The global transition to clean energy, explained in 12 charts” [Online]. Available: https://www.vox.com/energy-and-environment/2019/6/18/18681591/renewable-energy-china-solar-pv-jobs [Accessed: 22-Dec-2020].

[2] Chander, S., Purohit, A., Sharma, A., Nehra, S. P., & Dhaka, M. S. (2015). A study on photovoltaic parameters of mono-crystalline silicon solar cell with cell temperature. *Energy Reports*, *1*, 104-109.

[3] Carlson, D. E., Lin, G., & Ganguly, G. (2000, September). Temperature dependence of amorphous silicon solar cell PV parameters. In *Conference Record of the Twenty-Eighth IEEE Photovoltaic Specialists Conference-2000 (Cat. No. 00CH37036)* (pp. 707-712). IEEE.

[4] Thongpao, K., Sripadungtham, P., Raphisak, P., Sriprapha, K., & Hattha, E. (2010, May). Outdoor performance of polycrystalline and amorphous silicon solar cells based on the influence of irradiance and module temperature in Thailand. In *ECTI-CON2010: The 2010 ECTI International Confernce on Electrical Engineering/Electronics, Computer, Telecommunications and Information Technology* (pp. 74-77). IEEE.

[5] Landis, G. A., Belgiovane, D. J., & Scheiman, D. A. (2011, June). Temperature coefficient of multijunction space solar cells as a function of concentration. In *2011 37th IEEE Photovoltaic Specialists Conference* (pp. 001583-001588). IEEE.

[6] Singh, P., & Ravindra, N. M. (2012). Temperature dependence of solar cell performance—an analysis. *Solar energy materials and solar cells*, *101*, 36-45.

[7] Or, A. B., & Appelbaum, J. (2014). Dependence of multi-junction solar cells parameters on concentration and temperature. *Solar Energy Materials and Solar Cells*, *130*, 234-240.

[8] Fathi, M., Abderrezek, M., Djahli, F., & Ayad, M. (2015). Study of thin film solar cells in high temperature condition. *Energy Procedia*, *74*, 1410-1417.

[9] Belhocine-Nemmar, F., Belkaid, M. S., Hatem, D., & Boughias, O. (2010). Temperature effect on the organic solar cells parameters. *International Journal of Chemical and Molecular Engineering*, *4*(4), 257-259.

[10] Chirvase, D., Chiguvare, Z., Knipper, M., Parisi, J., Dyakonov, V., & Hummelen, J. C. (2003). Temperature dependent characteristics of poly (3 hexylthiophene)-fullerene based heterojunction organic solar cells. *Journal of Applied Physics*, *93*(6), 3376-3383.

[11] Cojocaru, L., Uchida, S., Sanehira, Y., Gonzalez-Pedro, V., Bisquert, J., Nakazaki, J., ... & Segawa, H. (2015). Temperature effects on the photovoltaic performance of planar structure perovskite solar cells. *Chemistry Letters*, *44*(11), 1557-1559.

[12] Speirs, M. J., Dirin, D. N., Abdu-Aguye, M., Balazs, D. M., Kovalenko, M. V., & Loi, M. A. (2016). Temperature dependent behaviour of lead sulfide quantum dot solar cells and films. *Energy & Environmental Science*, *9*(9), 2916-2924.

[13] Xing, M., Zhang, Y., Shen, Q., & Wang, R. (2020). Temperature dependent photovoltaic performance of TiO2/PbS heterojunction quantum dot solar cells. *Solar Energy*, *195*, 1-5.

[14] Abderrezek, M., Fathi, M., & Djahli, F. (2018). Comparative Study of Temperature Effect on Thin Film Solar Cells.

[15] Silverman, T. J., Deceglie, M. G., Marion, B., Cowley, S., Kayes, B., & Kurtz, S. (2013, June). Outdoor performance of a thin-film gallium-arsenide photovoltaic module. In *2013 IEEE 39th Photovoltaic Specialists Conference (PVSC)* (pp. 0103-0108). IEEE.

[16] Raga, S. R., & Fabregat-Santiago, F. (2013). Temperature effects in dye-sensitized solar cells. *Physical Chemistry Chemical Physics*, *15*(7), 2328-2336.

[17] Kalogirou, S. (Ed.). (2017). *McEvoy's handbook of photovoltaics: fundamentals and applications*. Academic Press

[18] “Photovoltaic Effect” [Online]. Available: https://energyeducation.ca/encyclopedia/Photovoltaic_effect [Accessed: 23-Dec-2020].
.

[19] Green, M. A. (1990). Intrinsic concentration, effective densities of states, and effective mass in silicon. *Journal of Applied Physics*, *67*(6), 2944-2954.

[20] Cubas, J., Pindado, S., & De Manuel, C. (2014). Explicit expressions for solar panel equivalent circuit parameters based on analytical formulation and the Lambert W-function. *Energies*, *7*(7), 4098-4115.

[21] “IV Curve” [Online]. Available: https://www.pveducation.org/pvcdrom/solar-cell-operation/iv-curve [Accessed: 23-Dec-2020].

[22] Sabry, M., & Ghitas, A. E. (2007). Influence of temperature on methods for determining silicon solar cell series resistance.

[23] Sahin, G. (2016). Effect of temperature on the series and shunt resistance of a silicon solar cell under frequency modulation. *Journal of Basic and Applied Physics*, *5*(1), 21-29.

[24] Khanna, S., Sundaram, S., Reddy, K. S., & Mallick, T. K. (2017). Performance analysis of perovskite and dye-sensitized solar cells under varying operating conditions and comparison with monocrystalline silicon cell. *Applied Thermal Engineering*, *127*, 559-565.

[25] Li, H. H. (1980). Refractive index of silicon and germanium and its wavelength and temperature derivatives. *Journal of Physical and Chemical Reference Data*, *9*(3), 561-658.

[26] Jellison Jr, G. E., & Burke, H. H. (1986). The temperature dependence of the refractive index of silicon at elevated temperatures at several laser wavelengths. *Journal of applied physics*, *60*(2), 841-843.

[27] Sun, B. K., Zhang, X., & Grigoropoulos, C. P. (1997). Spectral optical functions of silicon in the range of 1.13-4.96 eV at elevated temperatures. *International Journal of Heat and Mass Transfer*, *40*(7), 1591-1600.

[28] Jellison Jr, G. E., & Modine, F. A. (1994). Optical functions of silicon at elevated temperatures. *Journal of Applied Physics*, *76*(6), 3758-3761.

[29] Mustapha, M., Fudholi, A., Yen, C. H., Ruslan, M. H., & Sopian, K. (2018). Review on energy and exergy analysis of air and water based photovoltaic thermal (PVT) collector. *International Journal of Power Electronics and Drive Systems*, *9*(3), 1367.

[30] Tonui, J. K., & Tripanagnostopoulos, Y. (2007). Improved PV/T solar collectors with heat extraction by forced or natural air circulation. *Renewable energy*, *32*(4), 623-637.

[31] Ramos, F., Cardoso, A., & Alcaso, A. (2010, February). Hybrid photovoltaic-thermal collectors: A review. In *Doctoral Conference on Computing, Electrical and Industrial Systems* (pp. 477-484). Springer, Berlin, Heidelberg.

[32] Chandel, S. S., & Agarwal, T. (2017). Review of cooling techniques using phase change materials for enhancing efficiency of photovoltaic power systems. *Renewable and Sustainable Energy Reviews*, *73*, 1342-1351.

[33] Siecker, J., Kusakana, K., & Numbi, B. P. (2017). A review of solar photovoltaic systems cooling technologies. *Renewable and Sustainable Energy Reviews*, *79*, 192-203.

[34] Abdulgafar, S. A., Omar, O. S., & Yousif, K. M. (2014). Improving the efficiency of polycrystalline solar panel via water immersion method. *International Journal of Innovative Research in Science, Engineering and Technology*, *3*(1), 96-101.

[35] Krauter, S. (2004). Increased electrical yield via water flow over the front of photovoltaic panels. *Solar energy materials and solar cells*, *82*(1-2), 131-137.

[36] Zhu, L., Raman, A. P., & Fan, S. (2015). Radiative cooling of solar absorbers using a visibly transparent photonic crystal thermal blackbody. *Proceedings of the national academy of sciences*, *112*(40), 12282-12287.

[37] Borkar, D. S., Prayagi, S. V., & Gotmare, J. (2014). Performance evaluation of photovoltaic solar panel using thermoelectric cooling. *International Journal of Engineering Research*, *3*(9), 536-539.

[38] Kumar, R. S., Priyadharshini, N. P., & Natarajan, E. (2015). Experimental and numerical analysis of photovoltaic solar panel using thermoelectric cooling. *Indian Journal of Science and Technology*, *8*(36), 252-256.

Appendix

Semiconductor's Data

Table A-1 Silicon material proprieties

Relative permittivity	11.7
Electron lifetime, SRH (s)	1e-5
Hole lifetime, SRH (s)	1e-5
Band gap (eV)	1.12
Electron affinity (eV)	4.05
Effective density of states, valence band (1/cm³)	1.04e19
Effective density of states, conduction band (1/cm³)	2.8e19
Electron mobility (cm²/(V·s))	1450
Hole mobility (cm²/(V·s))	500

Table A-2 $CuInSe_2$ material proprieties

Relative permittivity	15.2
Electron lifetime, SRH (s)	1e-6
Hole lifetime, SRH (s)	1e-6
Band gap (eV)	1.02
Electron affinity (eV)	4.6
Effective density of states, valence band (1/cm³)	1.66e20
Effective density of states, conduction band (1/cm³)	6.77e18
Electron mobility (cm²/(V·s))	1000
Hole mobility (cm²/(V·s))	50

Table A-3 CdTe material proprieties

Relative permittivity	10.2
Electron lifetime, SRH (s)	220e-9
Hole lifetime, SRH (s)	1e-5
Band gap (eV)	1.5
Electron affinity (eV)	4.28
Effective density of states, valence band (1/cm³)	1.27e19
Effective density of states, conduction band (1/cm³)	9.96e18
Electron mobility (cm²/(V·s))	1450
Hole mobility (cm²/(V·s))	100

Table A-4 $CH_3NH_3PbI_3$ material proprieties

Relative permittivity	5.76
Electron lifetime, SRH (s)	1e-6
Hole lifetime, SRH (s)	1e-6
Band gap (eV)	1.52
Electron affinity (eV)	3.6
Effective density of states, valence band (1/cm³)	3.92e19
Effective density of states, conduction band (1/cm³)	2.77e19
Electron mobility (cm²/(V·s))	67
Hole mobility (cm²/(V·s))	67